Preprints (www.preprints.org) | NOT PEER-REVIEWED | Posted: 7 December 2020 doi:10.20944/preprints202012.0140.v1

Article

Effect of helix angle on the performance of Helical Vertical axis wind turbine

Unnikrishnan Divakaran [1], Ajith Ramesh [1], Akram Mohammad[2] and Ratna Kishore Velamati [1,*]

[1] Department of Mechanical Engineering, Amrita School of Engineering, Amrita Vishwa Vidyapeetham, Coimbatore, India.; d_unnikrishnan@cb.amrita.edu, r_ajith@cb.amrita.edu, v_ratnakishore@cb.amrita.edu
[2] Department of Aeronautical Engineering, King Abdulaziz University, Jeddah, Saudi Arabia.; ammohamad4@kau.edu.sa
* v_ratnakishore@cb.amrita.edu

Abstract: The global energy crisis has lead researchers explore other sources of energy like wind, resulting in a wide acceptance of wind turbines. Vertical axis wind turbines (VAWT) more suitable for small scale application in urban conditions than their horizontal-axis counterparts. A Helical bladed VAWT would reduce the ripple effect when compared to Straight bladed VAWT. The effect of the blade helix angle on the aerodynamic performance of VAWT using 3D numerical simulations is studied. Turbulence modelled using 4-Equation transition SST k-w model. Three different helix angles of 60°, 90° and 120° of a 3 bladed VAWT operating across different tip speed ratios were studied. The 60° helical bladed VAWT was found to perform better than all other helical bladed and straight bladed VAWT. Standard deviation of the moment coefficient generated by a blade plotted against 360 of azimuth rotation revealed that the ripple effect on the shaft produced by cyclic loading of the straight blade is considerably reduced upon introduction of helix angle, with 120° helical blade giving lowest standard deviation. The analysis has been done for the percentage of power generated by each quartile of flow and the contribution of each section of the blade. A comparative study was also conducted between different helical bladed VAWT and straight bladed VAWT. Flow feature analysis also revealed the reasons behind secondary peaks and the performance improvement when tip speed ratio increases. Wake structure analysis and flow contours were also studied for a better understanding of the flow field.

Keywords: Vertical Axis Wind Turbine; Wind Energy; Helical Blade

---

1. Introduction

Unhindered access to electric power is one of the most important factors ensuring the dynamic development of the countries and civilisations. Since the start of 20th-century fossil fuels have been considered as the most common energy carrier which has caused a rapid growth of civilisation. However, due to ecological and economic issues, many countries are introducing new regulations to cut down the utilization of fossil fuels and emission of CO_2 [1][2][3]. According to these regulations, most of the states have committed to increasing a percentage of the renewable sources of energy in the total installed electric power generation capacity. The wind energy can be a good alternative for fossil fuels as it can help in reducing the consumption of fossil fuels and emission of flue gasses. The main disadvantage of the utilisation of wind energy is its high sensitivity to the forecast conditions[4][5]. This disadvantage makes it difficult to control and foresee wind energy production. Other disadvantages are noise generated by wind turbines[6], their visual[7] and environmental [8](behaviour of animals, especially birds) impact on the surrounding. Also, erection of large-scale wind farm has effects on wind flow pattern and precipitation in the long term [9]. Some of the above problems can be overcome by decentralised application of vertical axis wind turbines (VAWTs), which are less sensitive to the wind conditions and have a broader range of operational wind speed. Moreover, there are certain studies which prove that the performance of VAWTs are not limited to

Betz number[10][11]; hence, units with efficiency higher than traditional horizontal axis wind turbines may be realised.

VAWTs are more apt to be used in an urban environment because of the following reasons: lower noise emission, higher cut off wind speed, lower minimum operational wind speed, low susceptibility to the turbulence level of the wind, omnidirectionality, and compact construction[12][13]. Because of these reasons, there is growing interest and research (experimental and numerical) in VAWTs. However, there is still a lot to explore to attain the level of development comparable to the HAWTs.

VAWTs are broadly classified based on their prime motive force: lift (Darrieus turbines) and drag (Savonious turbines). Savoniuos turbines are suitable for low tip speed ratio (TSR) conditions, and better self-starting, but their power coefficient is low when compared with similar Darrius turbines. On the other hand, Darrieus VAWTs perform better at higher TSRs, and are unaffected by lateral winds but have self-starting issues and structural loading problems due to cyclic forces. Blades employed in lift based VAWTs are of varied shapes: straight, Troposkien (Egg-beater shape), Helical, canted, Tulip shaped, Butterfly shaped, etc. These nonstraight blade designs can improve the structural issues of the turbine.

Though the non-straight blades may answer structural issues, understanding of the flow across the turbine is also critical to the improvement of the turbine's performance. The study of flow across a turbine is complex and causes phenomenon like dynamic-stall. The flow past airfoil which changes the attack angle is yet another phenomenon that needs through investigation. Knowledge of these phenomena would help understand the aerodynamics of the turbine and hence improve their performance. The geometric parameters like solidity, pitch angle and airfoil shape, and operational parameters like Reynolds number, turbulence intensity, and TSR affect the turbine performance. Various researches, on straight blade VAWT, have extensively studied geometric parameters like solidity[14][15][16][17], pitch angle[18][19][20], and airfoil shape[21][22][23]. Similarly, the operational parameters of a straight blade VAWT like TSR [24][25], Turbulence intensity[26][27] and Reynolds number of operation[16][25][28] are also comprehensively studied.

Recently research in non-straight blade VAWT has gained momentum. Blade shapes like Helical[29][30][31], Troposkien[32][33][34][35][36], V-Shaped[37], and Hybrid[38] have been studied by various researchers for its structural integrity. However, studies on to the effect of these geometrical parameters on the aerodynamic performance of non-straight bladed VAWT's are limited. Numerical and experimental study by Battisti et al. [32] on straight blade and troposkien blade turbines of similar swept area resulted in benchmarking the performance of these turbines. The review was mostly about the performance of small scale turbines under different operating conditions which led to a better understanding of the flow features that affected the incoming blade. Lee and Lim [39]in their numerical study on the effect of variying helix angles (0° to 30°) of the blades of VAWT (chord of 150 mm) (height 600 mm) (rotor diameter of 740 mm) concluded that the helix angle does not contribute to the improvement of the performance of the turbine. In another study by Scheurich[40], on the effect of blade curvature and helix angle it was concluded that for a better understanding of the aerodynamic effects of a non-straight blade, it is essential to analyse the interactions of wakes of the nonstraight blade of a VAWT. A numerical study comparing a part blade VAWT to a helical VAWT by Karimian and Abdolahifar [41] focused on the effect of segmented blades which perform like the helical blade. The study on the performance characterisation of these turbines operating under different TSRs concluded by defending the 3-part blade model to be more effective at lower TSR, and giving better self-starting capabilities.

Although there have been studies on helical bladed VAWT, the unavailability of analytical research on commercial-scale VAWTs and the effect of change in helix angle on the aerodynamic performance of a VAWT are the motivation behind this work. Researches in helical bladed VAWT focus mostly on their aerodynamic study under altering TSR[29][30][31] and changing helix angles[37][42][43][44]. However, those studies are limited to maximum helix angles of 135° and are limited to lab-scale models. A study based on commercial small scale turbines is essential as it can help the development and implementation of VAWT in situ. The objective of this work is to understand the effect of varying helix angles (60° to 120°) on the performance of VAWT under different operating conditions of TSR. The study also tries to compare the performance of these helical turbines to a straight blade VAWT of similar swept area. The primary effects on the aerodynamic performance and the continuity of power generated from the turbines are analysed. Effect of helix angle on the loads on various section of the blade is also studied in detail.

2. Problem Statement

The purpose of the study is to investigate the effect of helical angles on the aerodynamic performance of a helical VAWT. Straight bladed VAWT have a ripple effect on the shaft. The ripple nature of the loading comes because of the limited operating zone of a blade during its entire cycle. The cyclic nature of loading on the wind turbine shaft causes critical failures in the structure. Hence increasing the operating angle of each blade was found to be a possible solution.

For this study, blade geometry is generated by helically extruding NACA0015 airfoil with no pitch. The airfoil is helically swept at 60°, 90° and 120° for obtaining the geometry. A shaft of 200 mm diameter is considered essential for better prediction of the flow field. Any cross-section of the turbine perpendicular to the axis of rotation, the area would be the standard airfoil with its centroid lying on the cylindrical surface generated by the rotation of the turbine. Although manufacturing of these helical blades is difficult using conventional manufacturing processes, contemporary techniques like additive manufacturing have laid the foundation for manufacturing near impossible geometries with ease and perfection. The blades have a chord of 210 mm length, the diameter of 1 m (leading to the solidity of 0.4) and the turbine has a height of 3 m. Since the blade has more extended azimuth angle of operation, the analysis of the turbine without the central shaft would lead to a wrong prediction of the flow field.

Figure 1 (a) shows the direction of rotation (θ) of the turbine and the definition of helix angle (ψ). The blue airfoil represents the bottom plane, and the red airfoil represents the top plane of the turbine. Figure 1 (b-d) represents the geometry of 60°, 90° and 120° helical bladed VAWT, respectively.

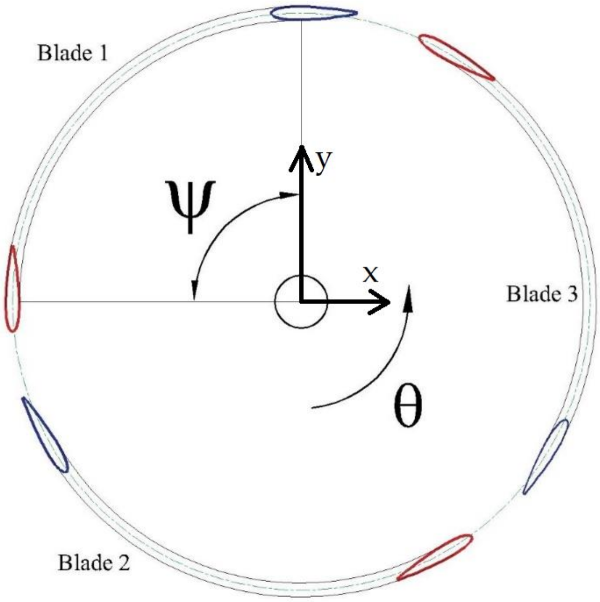

(a)

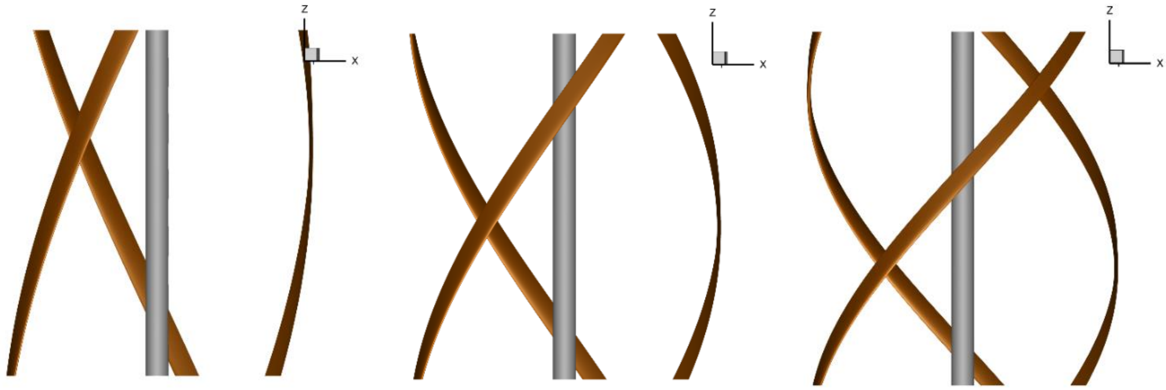

(b) (c) (d)

Figure 1. Top view of a Helical Blade VAWT with definition of direction of rotation (θ) and helix angle (ψ); front view of helical Blade VAWT (b) ψ = 60° (c) ψ = 90° (d) ψ = 120°

The inlet wind velocity is in the positive y-direction. Wind velocity direction is considered uniformly across all the analysis in this study.

3. Numerical Model

Flow across the turbine is always in the low Mach number range, hence it is a reasonable assumption to consider the flow to be incompressible. The conservation of mass (continuity), and Momentum (Navier-Stokes) equations, for a three-dimensional incompressible isothermal flow, is solved. Reynolds number of the flow over the blade is ranging from 1.4×10^5 to 3.5×10^5. Therefore the turbulence is modelled using transitional SST k-ω model. Rezaeiha et al.[45] have concluded that among all the turbulence models, Transition SST k- ω works better for VAWT simulations. Transition SST k- ω is used because the flow around VAWT is in transition regime, and it is difficult to characterise the flow to be either fully laminar or fully turbulent. The governing equations, i.e. conservation of mass (continuity) and Momentum (Navier-Stokes equations) used in the numerical modelling is as follows:

$$\nabla.\rho\vec{V} = 0 \tag{1}$$

$$\rho\frac{D\vec{V}}{Dt} = -\nabla p + \mu\nabla^2\vec{V} \tag{2}$$

$$\rho\left[\frac{\partial(k)}{\partial t} + \frac{\partial(\rho u_j k)}{\partial x_j}\right] = \hat{P}_k - \hat{D}_k + \frac{\partial}{\partial x_j}\left[(\mu + \sigma_k\mu_t)\frac{\partial k}{\partial x_j}\right] \tag{3}$$

$$\rho\left[\frac{\partial(\omega)}{\partial t} + \frac{\partial(u_j\omega)}{\partial x_j}\right] = P_\omega - D_\omega + \frac{\partial}{\partial x_j}\left[(\mu + \sigma_\omega\mu_t)\frac{\partial \omega}{\partial x_j}\right] + 2(1-F_1)\frac{\rho\sigma_{\omega 2}}{\omega}\frac{\partial k}{\partial x_j}\frac{\partial \omega}{\partial x_j} \tag{4}$$

$$\rho\left[\frac{\partial(\gamma)}{\partial t} + \frac{\partial(\rho u_j\gamma)}{\partial x_j}\right] = P_\gamma - D_\gamma + \frac{\partial}{\partial x_j}\left[(\mu + \frac{\mu_t}{\sigma_f})\frac{\partial \gamma}{\partial x_j}\right] \tag{5}$$

$$\rho\left[\frac{\partial(\hat{Re}_\alpha)}{\partial t} + \frac{\partial(u_j\hat{Re}_\alpha)}{\partial x_j}\right] = P_\alpha + \frac{\partial}{\partial x_j}\left[\sigma_\alpha(\mu + \mu_t)\frac{\partial \hat{Re}_\alpha}{\partial x_j}\right] \tag{6}$$

Where ρ is the density, V is the velocity, μ is the dynamic viscosity, p is the pressure, $\hat{P}_k, P_\omega, P_\gamma, P_{\theta t}$ are the production terms for respective quantities, $\hat{D}_k, D_\omega, D_\gamma$ are destruction terms of the respective quantities.

3.1. Computational Domain and Grid

The numerical domain is divided into two; stationary and rotating domain with mesh interface defined for proper continuity. The rectangular stationary domain shown in figure 2. has

Preprints (www.preprints.org) | NOT PEER-REVIEWED | Posted: 7 December 2020 doi:10.20944/preprints202012.0140.v1

been defined based on the reference value of turbine diameter D, with 15D length in the upwind and 30D in the downwind measured from the shaft centre. A width of 40D was defined to avoid any wall blockage effects. The height of 4.5 times the turbine diameter was defined for the domain. The rotating domain with mesh motion was defined to be three times the diameter of the turbine. Mesh in a section plane perpendicular to the turbine axis (z-axis) is shown in figure 3(a). It can be noticed that the rotating domain is given sufficient refinement to capture the flow fields near to the blades and shaft. Figure 3(b) shows the boundary layer of 2.5×10^{-5}m, which is defined near the blade walls. Controlled growth of mesh farther away from the blade is ensured by using various control volumes, as shown in Figure 3(c). In figure 3(b) the velocity inlet and pressure outlets are shown. The inlet velocity plane is from the centre of the turbine at a distance from 15 times the diameter of the turbine. The outlet pressure plane is at 30 times the diameter from the centre of the turbine at the downstream. The sidewalls and the top and bottom surfaces are defined to be free shear walls.

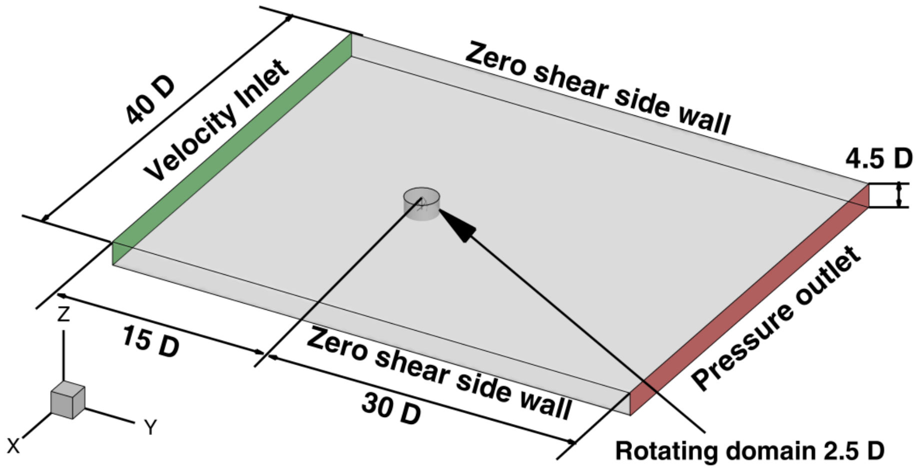

Figure 2. Domain consisting of the stationary cuboidal domain and rotating cylindrical domain

3.2. Boundary, Initial Conditions and computational procedure

The rectangular numerical domain considered consists of two side walls and top and bottom planes with zero shear. Inside of the rectangular domain, we have a cylindrical rotating domain which is interfaced with a sliding mesh interface. The rotating mesh is allowed to rotate about the z-axis, and the rotation is defined based on the tip speed ratio at which the simulations are run. It is determined by the formula: $N = \dfrac{60 \times TSR \times U_{\infty}}{2 \times \pi \times R}$ where N is the number of revolutions per second, TSR is the tip speed ratio, U_{∞} is the free stream velocity (10 m/s), and R is the radius of the turbine. It has to be noted that when the tip speed ratio is fixed, then the corresponding rotation for the rotating interface was defined. Hence the rotation of the domain for each simulation was defined depending on the TSR. The blades and shaft surfaces are defined as no slip. The top and bottom surfaces of the turbine blades are shaft are defined to compute the tip effects. The flow was initialised from the velocity inlet at 10 m/s. The rotation is initiated with and run for 10 cycles so that the results have converged. The time steps size was defined based on the rotation angle. Hence for each TSR, the time step size was defined.

The algorithm used for Pressure velocity coupling is COUPLED. The convective scheme employed is for spatial discretisation is second-order upwind scheme. The second order in time is used for transient terms. The under relaxation factor for turbulent kinetic energy, specific dissipation rate, intermittency and momentum thickness Re was set to 0.4. The turbulent viscosity under relaxation factor was set to be 0.5. For each time step, 40 iterations were performed such that the residuals for all the variables would converge to an order of 10^{-5}.

Preprints (www.preprints.org) | NOT PEER-REVIEWED | Posted: 7 December 2020 doi:10.20944/preprints202012.0140.v1

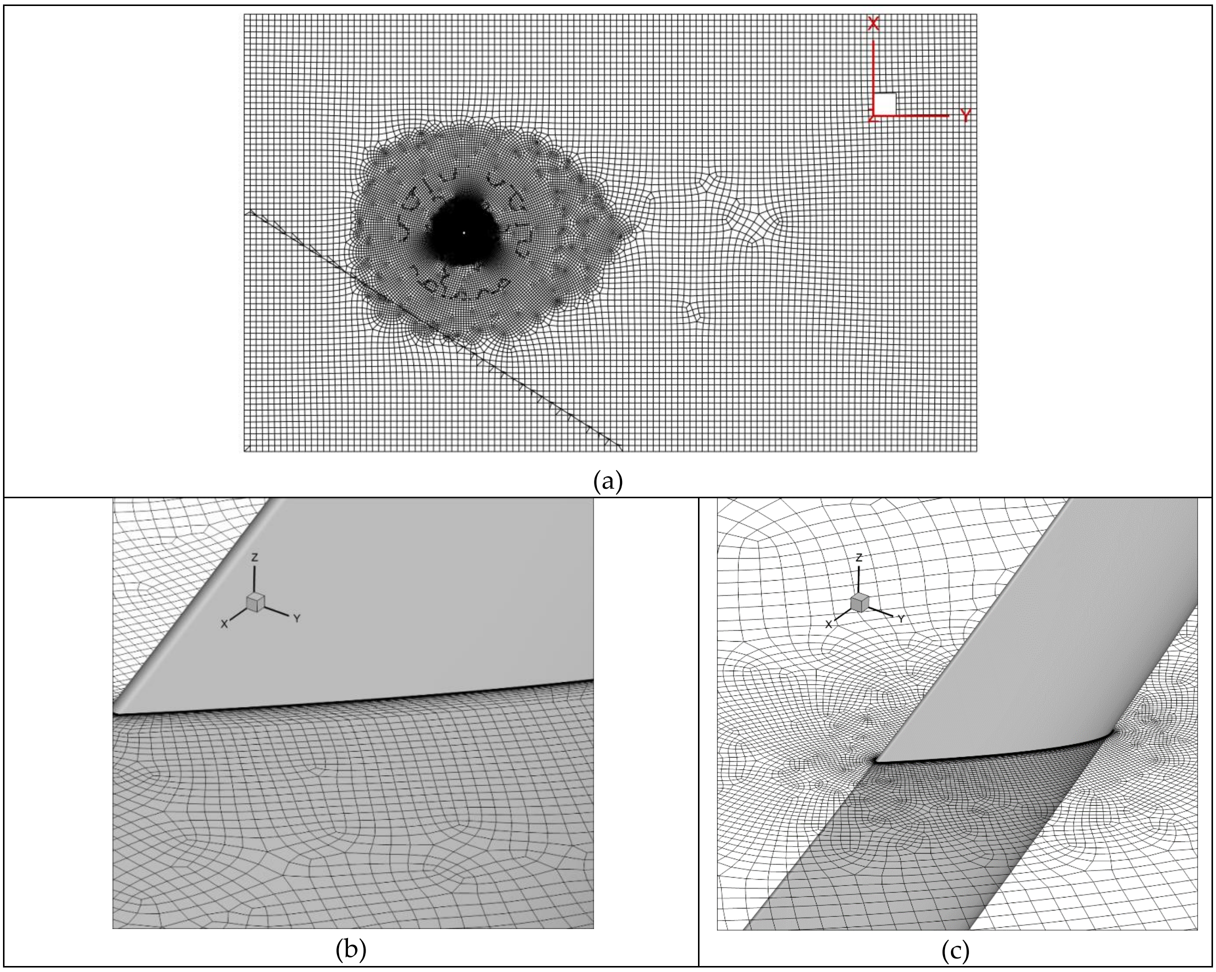

Figure 3. (a) Sectional view of the domain mesh (b) Mesh near the blade (c) Mesh Growth surrounding the blade

3.3. Model Validation and Solution Independence

Grid independence study is conducted in order to have consistency in the solution as well as reducing the computational effort. Three models of 9 million, 14 million and 21 million grid points were solved to get solution for 15 cyclic revolutions of the turbine. It can be seen from figure 4. (a) representing the moment coefficients of a single blade, that three grids are predicting similar results. Hence, for all the numerical calculations, the 9 million grid mesh was employed. The solutions were found to be in an agreeable range. The time resolution also plays a critical role. The time step was defined based on the azimuth angle of rotation of the turbine. Three different resolutions (2°, 1° and 0.5°) were tried and tested to make sure the results predicted are reasonable. From figure 4. (b) it is evident that all three-time step definitions are predicting similar solutions with significantly fewer errors.

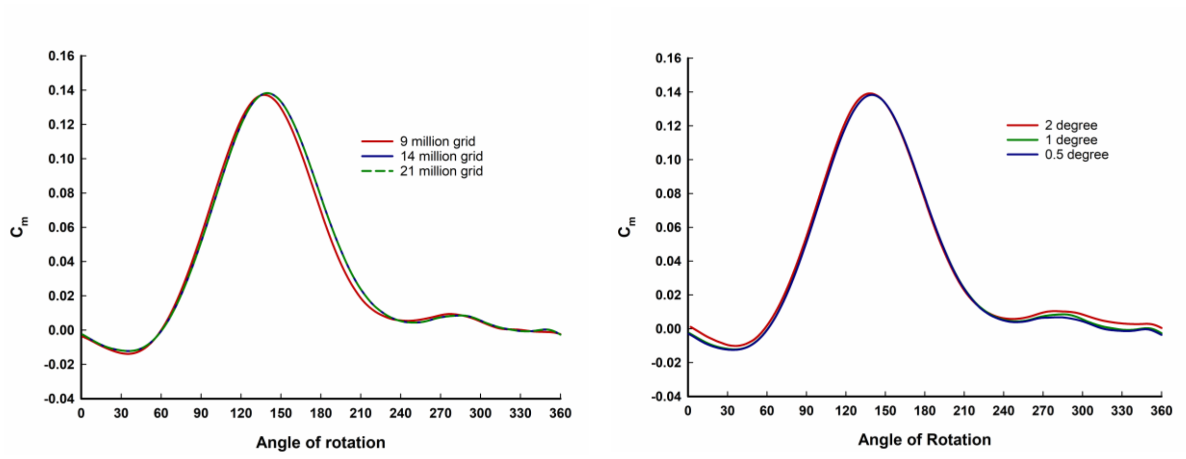

(a) (b)

Figure 4. Cm Plot for a single blade indicating (a) Grid independence (b) Time step independence

Figure 5. illustrates the cyclic convergence for a tip speed ratio of 2.3, 60° helical bladed VAWT case. The solution has achieved a cyclic nature by the end of the 10th cycle itself, which indicates that the solution has reached convergence. All the simulations were run for 14 rotation cycles of the turbine to remove any non-cyclic behaviour in the solution.

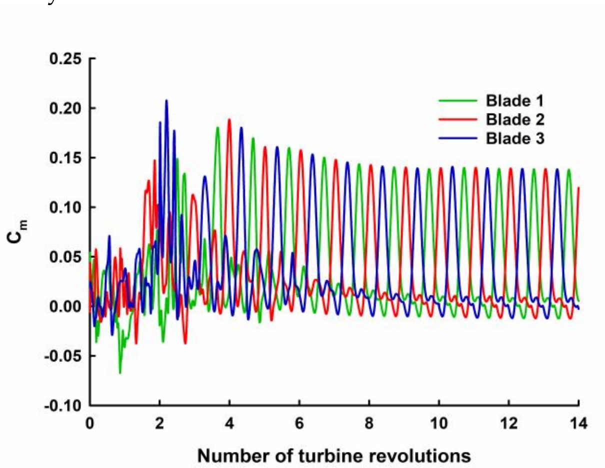

Figure 5. Cyclic convergence of solution for a 60° helical blade VAWT running at λ = 2.3

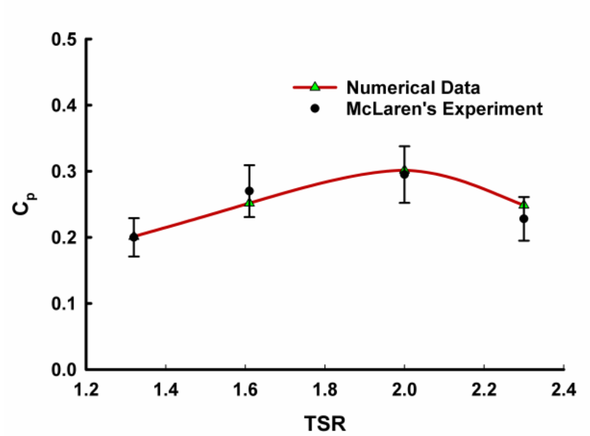

Figure 6. Validation of numerical results to McLarens experimental results

To validate the numerical model used in this study, McLaren's data was used. In the experimental study, a 420 mm chord 3 bladed straight VAWT was studied and tested in the wind tunnel. The numerical model with similar dimensions was simulated. The numerical results of the simulations deviated a maximum of 8%. This gave considerable confidence in the numerical model setting that is used in this study. Moreover, the percentage error reported by McLaren was ±14.5%. From figure 6, it is evident that the numerical results are well within the error bars of experimental results.

4. Results

4.1. Effect of Helix Angle on the performance of VAWT

Performance of vertical axis wind turbines for various helix angles operating over a range of tip speed ratio (TSR) is plotted in figure 7. Performance of straight blade VAWT and different helical VAWT are compared in this figure. It is seen that the straight blade VAWT showcases its best performance in lower TSR range (2.7 – 3), but when helix angle is introduced, the performance curve shows a shift in the peak maintaining a similar overall trend of the curve. For helix angle 60°, the performance is maximum at a TSR of 3.3 showcasing better performance compared to all other helical and straight blade turbines. For helix angles 90° and 120°, the performance is comparable with a straight blade turbine, but the performance is peaking at higher TSR. It is evident that the best performance is projected for 60° helical blade turbine, but the slope in the curve is too large for a small variation of TSR. For a 120° helical blade turbine, the performance curve looks much inferior to any other turbines that are considered.

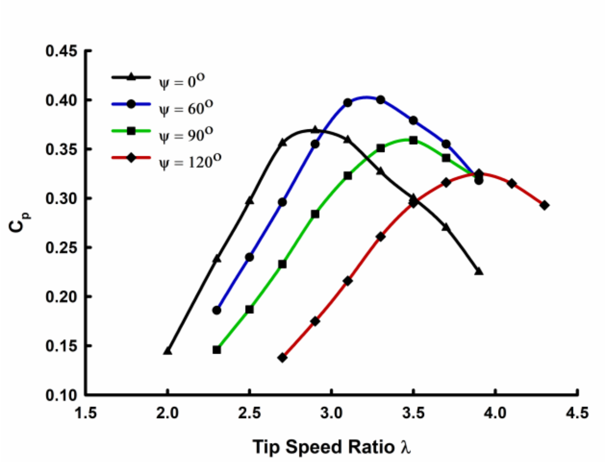

Figure 7. Coefficient of performance of VAWT for various helix angles

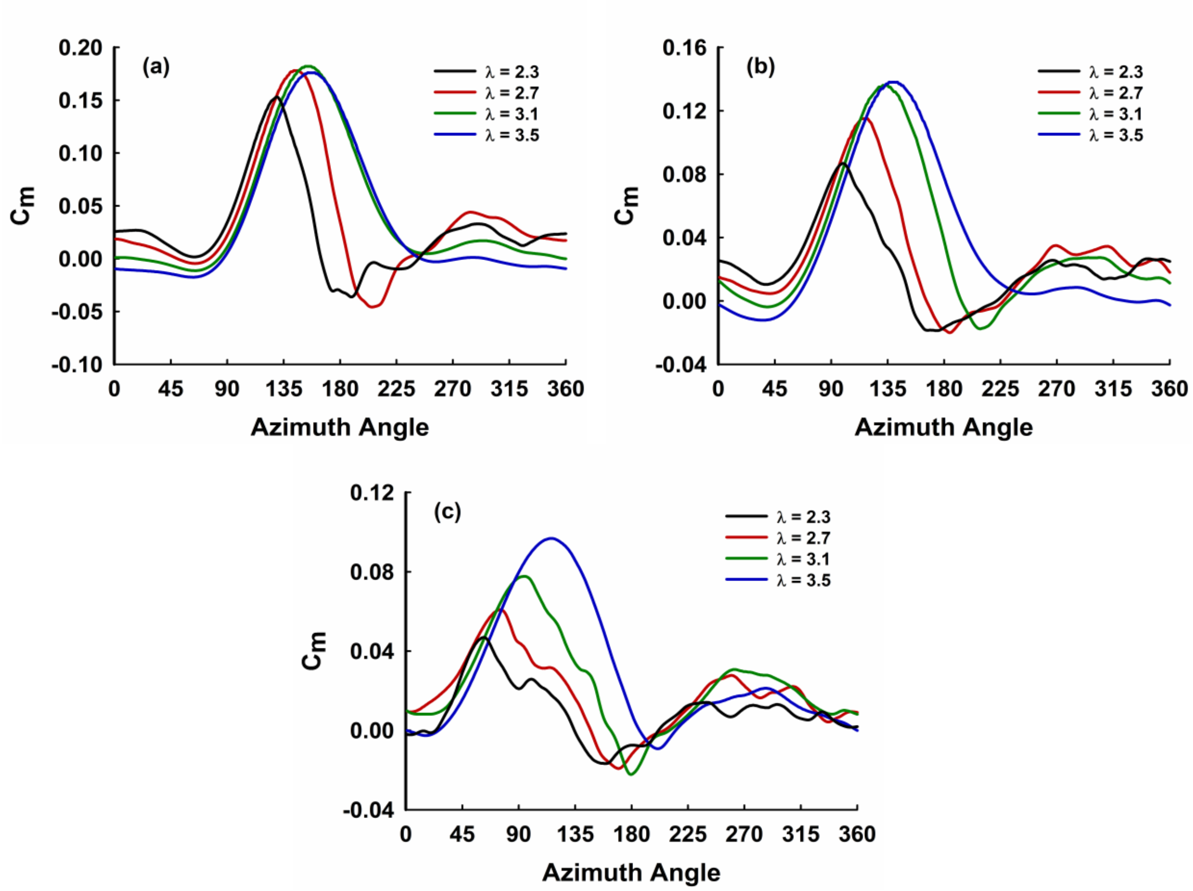

 doi:10.20944/preprints202012.0140.v1

Figure 8. Moment coefficient for various TSR, (a) helix angle 60° (b) helix angle 90°(c) helix angle 120°

The moment coefficient (C_m) of a single blade is plotted against the azimuthal angle of rotation in figure 8 (a-c) for helix angle 60°, 90° and 120° respectively. C_m curve at different TSR for different helix angles are plotted for each helical turbine. It should be noted that the coefficient of performance is the product of TSR and average C_m. Irrespective of helix angle, the peak performance of each blade keeps shifting to the higher azimuth angle as the TSR increases. As the helix angle increases, the shift in occouance in peak C_m is significant. For 60° helix angle the peak of C_m curve shifts in the range of 135° to 180° of azimuth angle for a TSR range of 2.3 to 3.5, whereas for 120° helical blade VAWT, the peak of C_m curve shifts from 45° to 135° of azimuth angle for the same range of TSR. This can be attributed to the reason that the increase in the helix angle would lead to exposure of blade to the incoming wind for larger azimuth angle. It is also interesting to see that the secondary peaks, which may be due to the significant reduction in wake interaction when TSR goes higher. The slope of the curve also increases as the helix angle decreases. This will have an adverse effect on the load that gets transmitted on to the shaft. A cross-comparison of helix angle (Figure 9. a - d) at λ = 2.3, 2.7, 3.1, 3.5 and 3.9 shows that straight blade VAWT had the highest peak and 120° Helical VAWT had the lowest peak. It is interesting to look at the curve slope for each helix angle blade. The curve is steep for lesser helix angle. To further investigate the effect of the slope of the curve on the performance, normalised cumulative C_m was plotted.

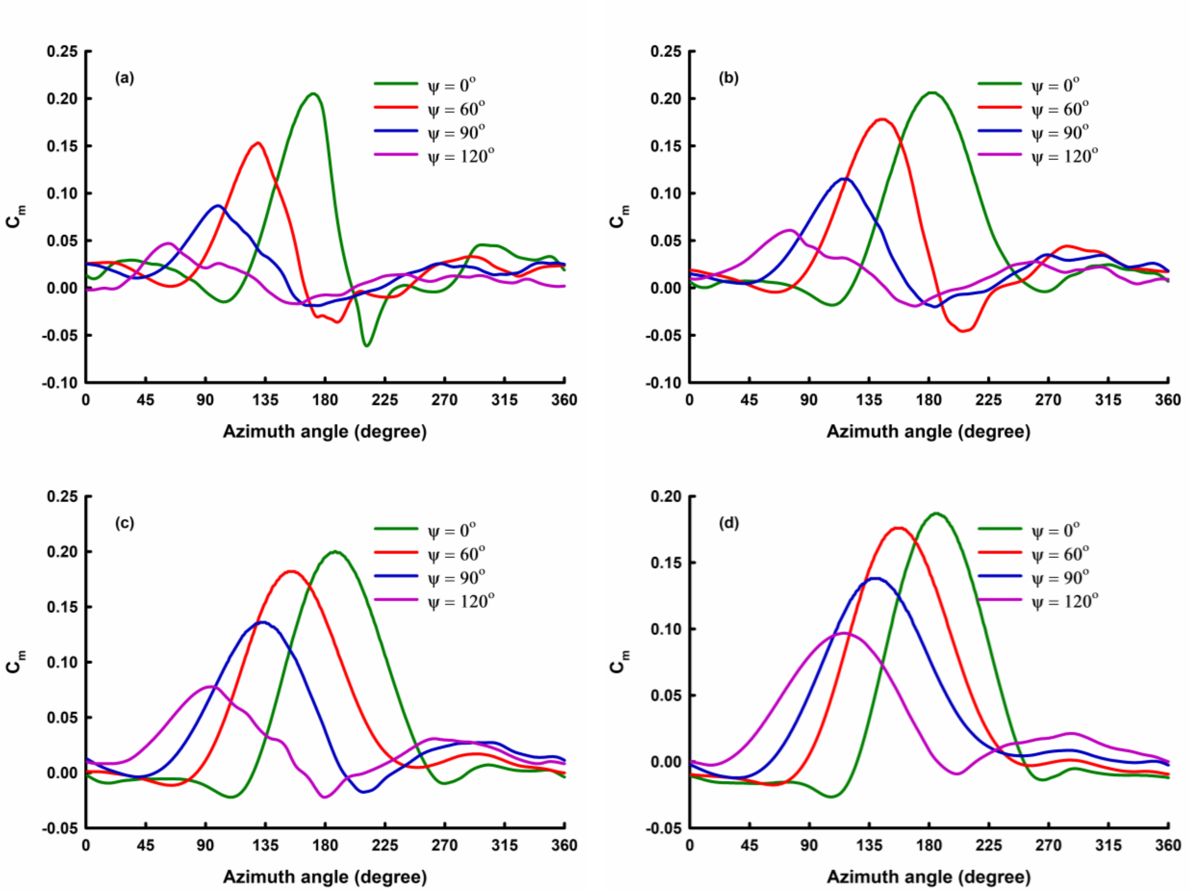

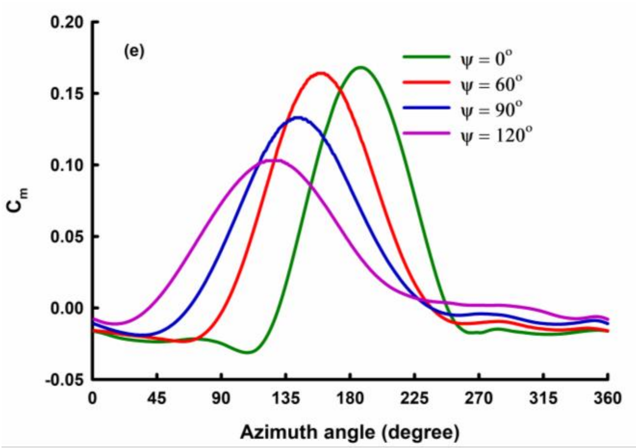

Figure 9. Cm curve for the first blade of straight 60°, 90° and 120° helix angle of blades compared at (a) λ = 2.3, (b) λ = 2.7, (c) λ = 3.1, (d) λ = 3.5, (e) λ = 3.9

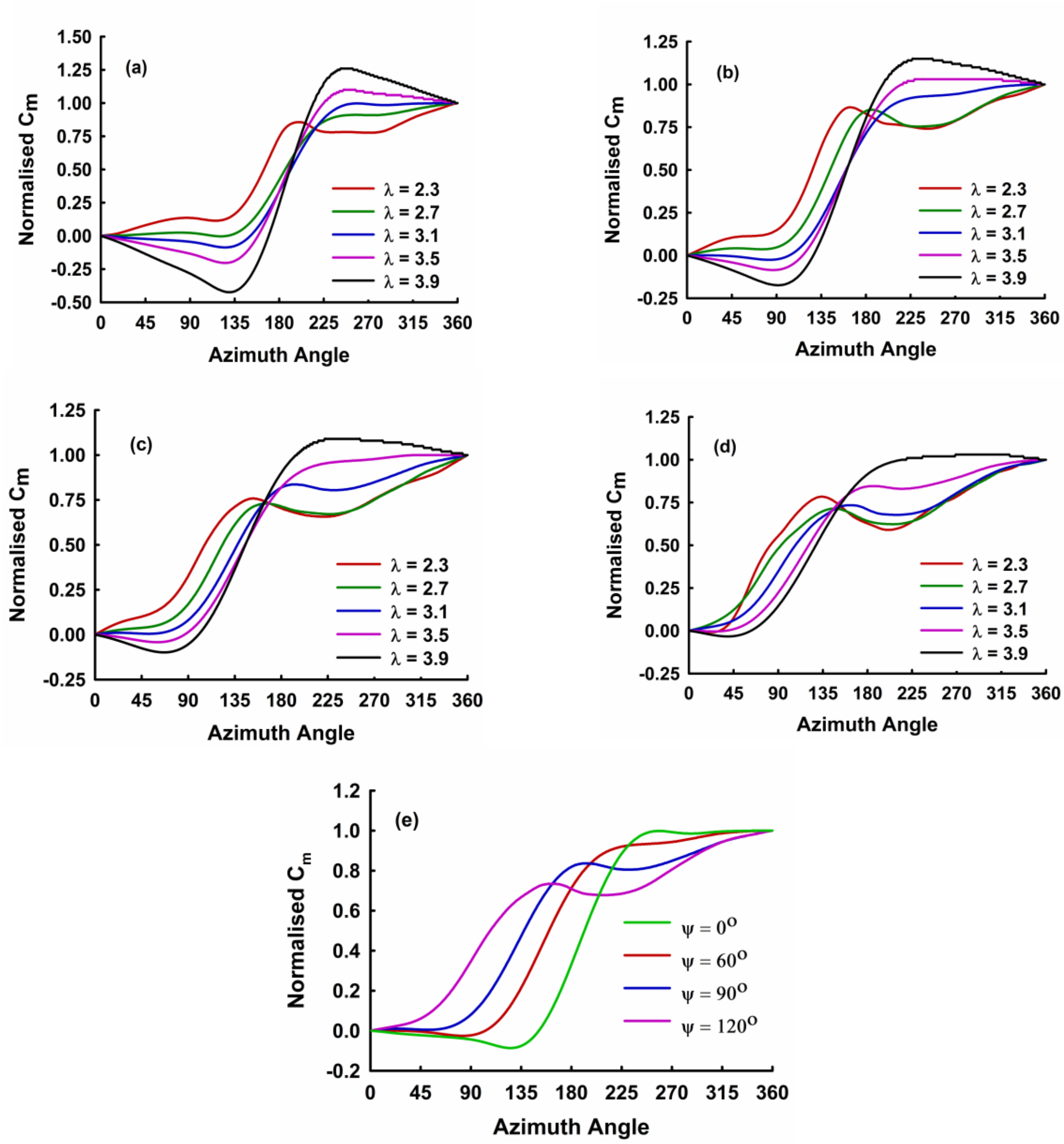

Figure 10. Normalised cumulatie Cm Curve of blade 1 at different l for (a) ψ = 0°, (b) ψ = 60° (c) ψ = 90°, (d) ψ = 120°, (e) Normalised curve of all helical bladed turbine compared against straight blade turbine at TSR of 3.1

In figure 10. the normalised curve was plotted, which gave a better understanding of the nature of energy generated. The trend of power generated in each of these cases was similar except that the slope of the curve was decreasing as the helix angle increases. This is attributed to the broader range of azimuth angle in which the power gets generated. It must be noted that the normalised curve also gave an understanding of how the trend behaved when the tip speed ratio was changed at different helix angles. When we compare the slope of cumulative C_m for different helix angle performing at the same TSR, the slope variation can be understood. The straight blade can be seen going to negative and then going above 1. This is mainly because of the limited azimuth angle of positive operation. Whereas the curve for 120° is having a lesser steep curve and most of the portion of the curve being positive. The negative slope in the cases of 90° and 120° are impressive because they represent the secondary wake interactions. It would be interesting to see the cumulative effect of all three blades on the turbine power generation curve. Hence the cumulative C_m curve as plotted in Figure 11.

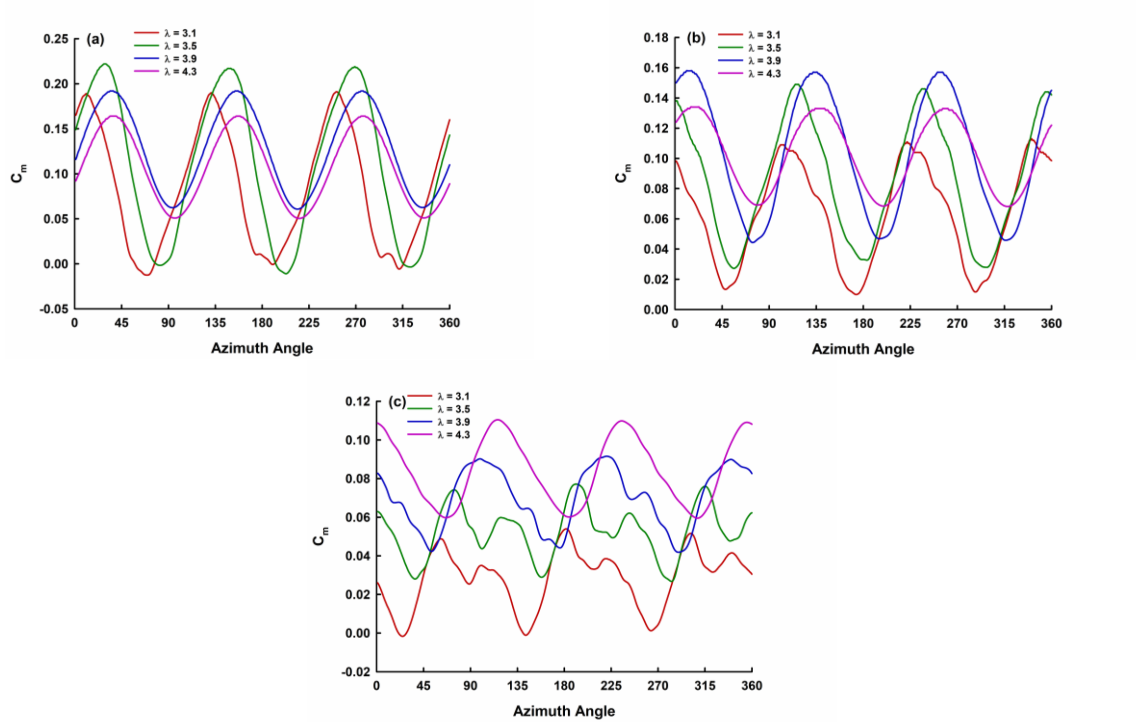

Figure 11. Cumulative C_m plot for helical turbine having (a) ψ = 60°, (b) ψ = 90° and (c) ψ = 120°

The cumulative C_m effect of each turbine was plotted for different tip speed ratios in figure 11. It was found that the C_m curve had a maximum point and a minimum point. These fluctuations in maximum and minimum are large for lower TSR for all the types of turbines. For 60° and 90° helical bladed turbines, it is noticed that the fluctuations minimise as the TSR increases. It is seen that for lower TSR the C_m curve has much instability for 120°a helical blade when operating at lower TSR. The possibility of wake interaction is higher since the blades have higher overlap in the circumference of the turbine.

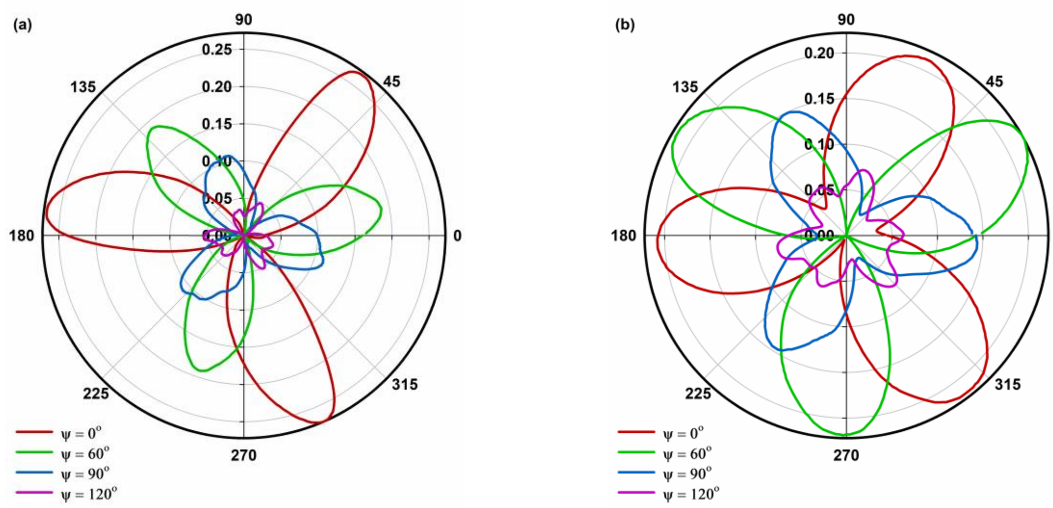

Preprints (www.preprints.org) | NOT PEER-REVIEWED | Posted: 7 December 2020 doi:10.20944/preprints202012.0140.v1

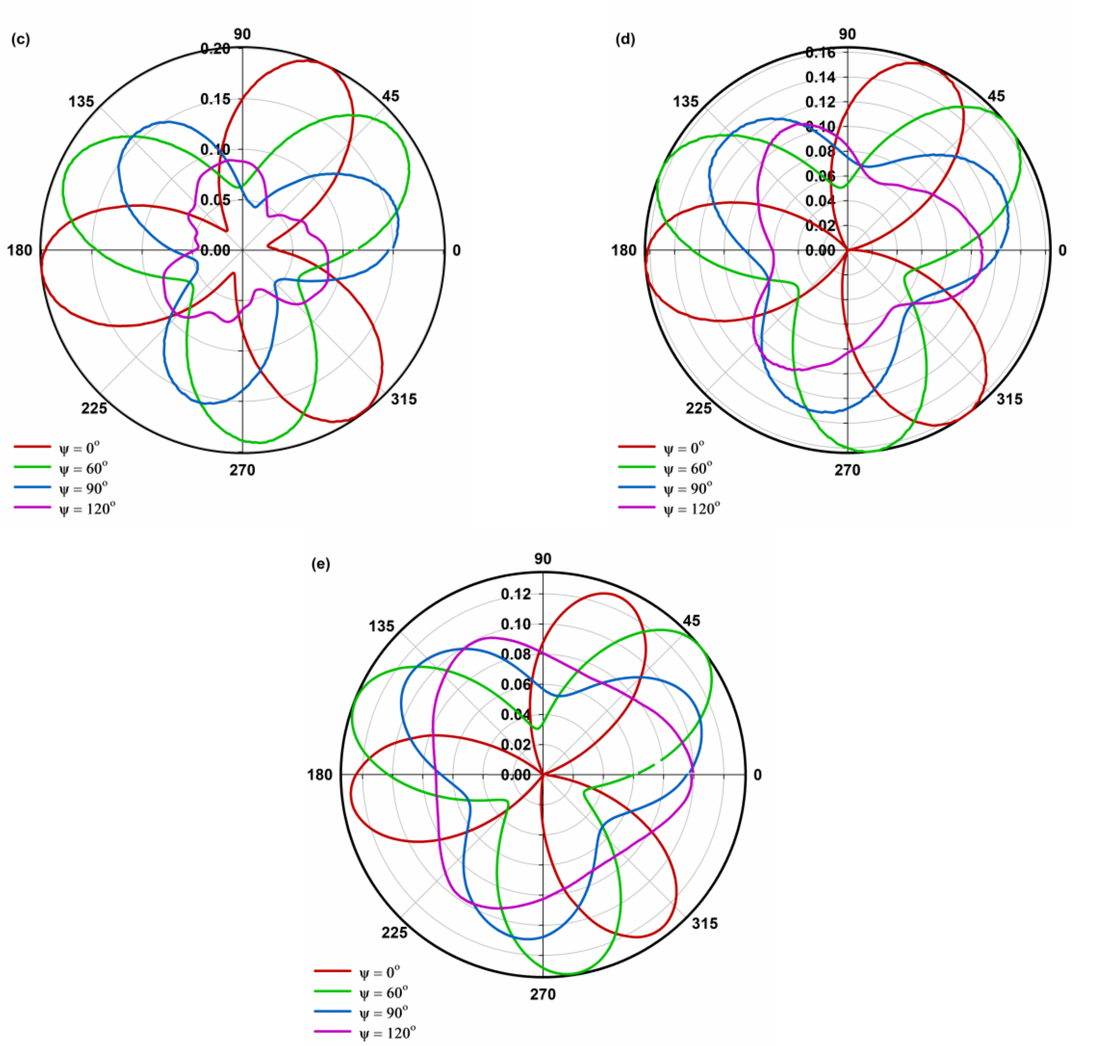

Figure 12. Cumilative polar plot of C_m comparing different helix angles and straight blade at (a)TSR = 2.3, (b) TSR = 2.5, (c) TSR = 3.1, (d) TSR = 3.5, (e) TSR = 3.9

The plot is trying to compare the performance of different helical bladed VAWT operating in the same TSR. However, the trends look quite similar for low and medium TSR, at Higher TSR the turbine having 120 helical bladed VAWT had a lesser deviation from the mean performance curve over the cycle

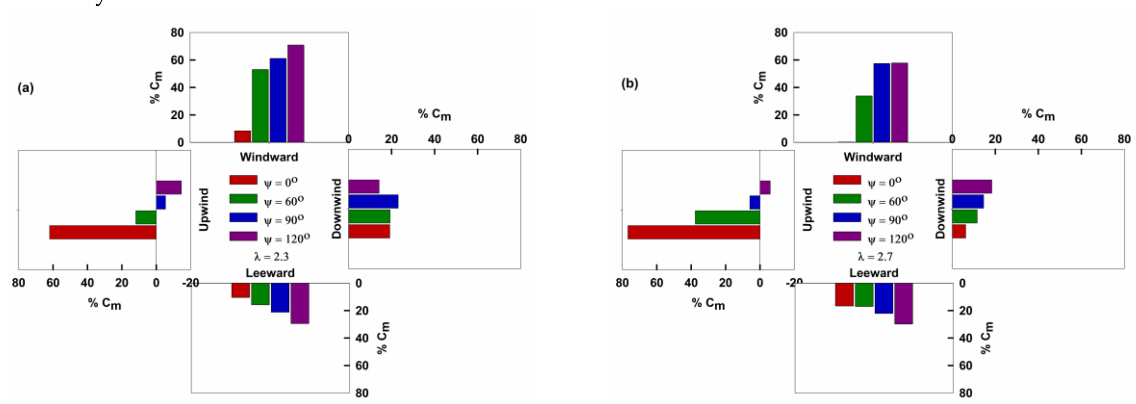

Preprints (www.preprints.org) | NOT PEER-REVIEWED | Posted: 7 December 2020 doi:10.20944/preprints202012.0140.v1

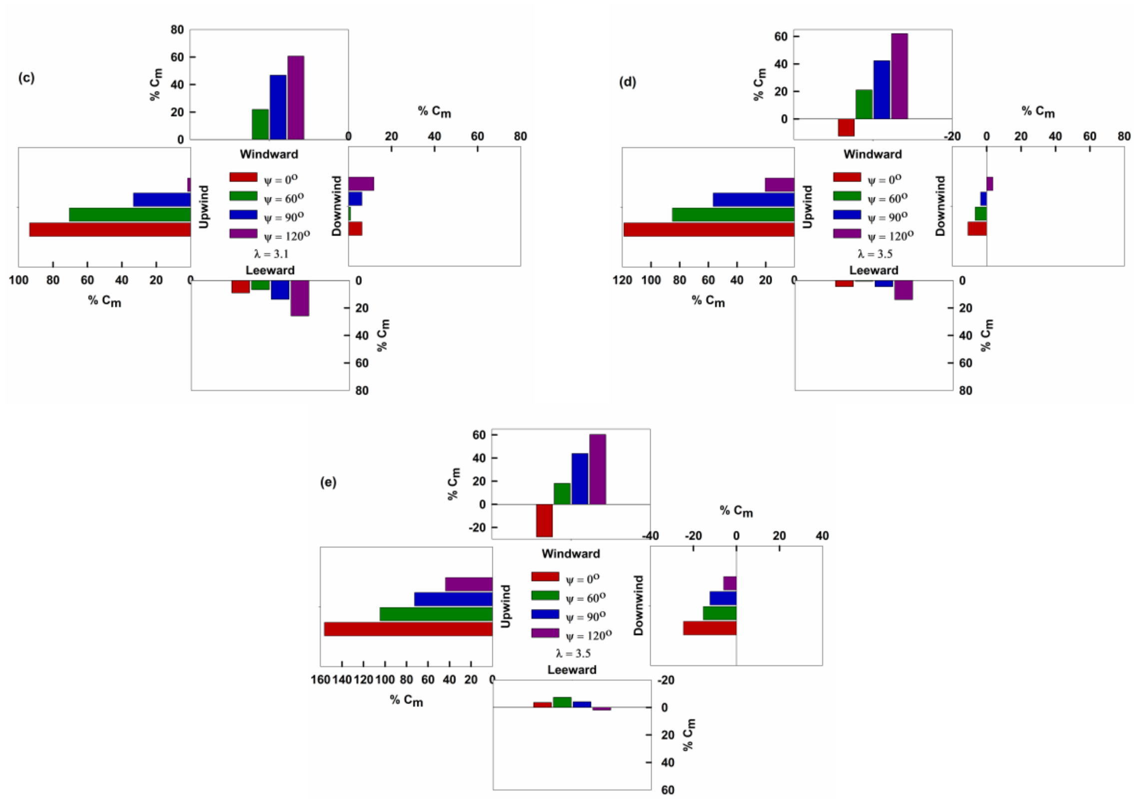

Figure 13. Percentage contribution by a blade in each quartile for all helical blade and straight blade at (a) TSR = 2.3, (b) TSR = 2.7, (c) TSR = 3.1, (d) TSR = 3.5 and (e) TSR = 3.9

In figure 12, the contribution of each turbine quartile in total power production is plotted to compare different helical turbines operating at TSR 2.3 to 3.9. The contribution is calculated as the difference between the cumulative sum of normalised C_m at the end and the start of each quartile. For several cases, it is seen that the percentage of contribution crosses 100%. This is mainly due to transitions from negative values of C_m at the beginning of the quartile to a more considerable positive value of C_m by the end of the quartile. It is also noticed that for such cases the percentage contribution of the blades will go into negative values in other quartiles as the total sum has to be 100%

It is interesting to note that the percentage contribution in the downwind side is positive for lower TSR. However, as the TSR increases the downwind quartile contribution tends to go to negative contributions. This can be attributed to the secondary wake interaction at the downstream of the flow at lower TSR. The leeward side of the flow also follows a similar trend and has interactions happening at lower TSR. At higher TSR, the difference in the contribution of each quartile becomes large for straight-bladed VAWT. Whereas the cumulative contribution of 120° helical blade VAWT shows positive contribution in all the quartiles. (Add percentage difference in the quartiles between 60 and 120) If we compare the contributions of each quartile for TSR = 2.3, it can be seen that almost all quartiles contribute positively except for 90° and 120°helical VAWT. Straight blade VAWT can be seen producing more than 100% in the upwind quartile for TSR>3.1. This explains the sudden increase in the slope of the normalised cumulative C_m curve. It can be concluded that when the helix angle is introduced, the nature of the power generated over the entire rotation of the turbine changes its characteristics.

Preprints (www.preprints.org) | NOT PEER-REVIEWED | Posted: 7 December 2020 doi:10.20944/preprints202012.0140.v1

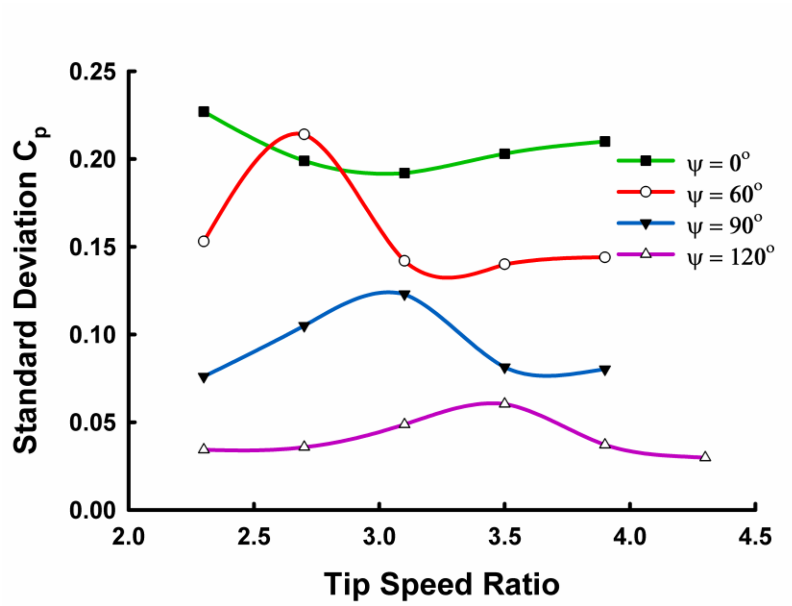

Figure 14. The Standard deviation of C_P of different helical bladed and straight bladed VAWT operating at different TSR

The ripple effect on the turbine shaft is understood much with the help of standard deviation of C_P plotted for different turbines operating at different TSR. Figure 13 represents the standard deviation of C_P of different types of helical bladed turbines and straight bladed turbine. The standard deviation reduces as the helix angle increases. The maximum deviation is for straight-bladed VAWT running at 2.3 TSR. For TSR 2.7, the standard deviation of 60° helical bladed VAWT overshot the straight-bladed VAWT. The standard deviation of C_P is much less for 120° helical bladed VAWT than any other configuration of blades. The standard deviation is highest for the straight-bladed VAWT. Straight blade shows maximum variation, and it is approximately 85% higher than the 120° helical bladed VAWT. The maximum standard deviation for a turbine is away from the peak performance of that turbine.

4.2. Effect of helix angle on turbine blade loads

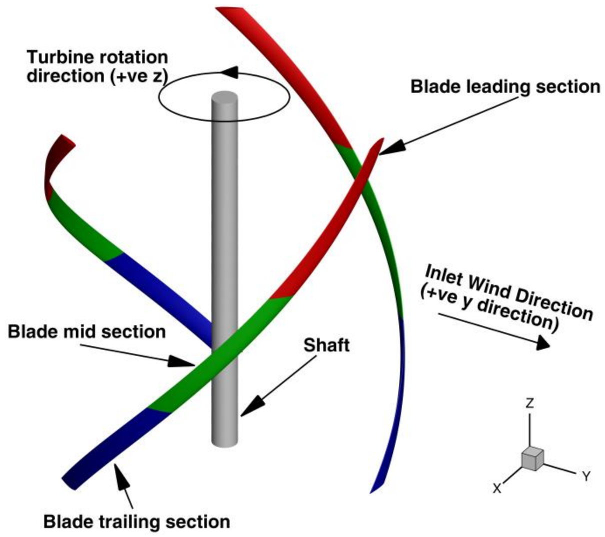

Figure 15. Sections of blades of a helical vertical axis wind turbine

To understand the power generation distributed across different quartiles of a turbine, it is essential to know how various part of a helical blade will generate the C_P. The blades were divided into 3 sections of equal height. The sections are named as leading, mid and trailing section, and they are represented in figure 15 with red, green and blue colours respectively. The leading section enters any of the quartile first followed by mid-section and trailing section while the turbine is in rotation. A sectional analysis is essential in this case as the blade is interacting with the flow continuously across different quadrants.

(a) (b)

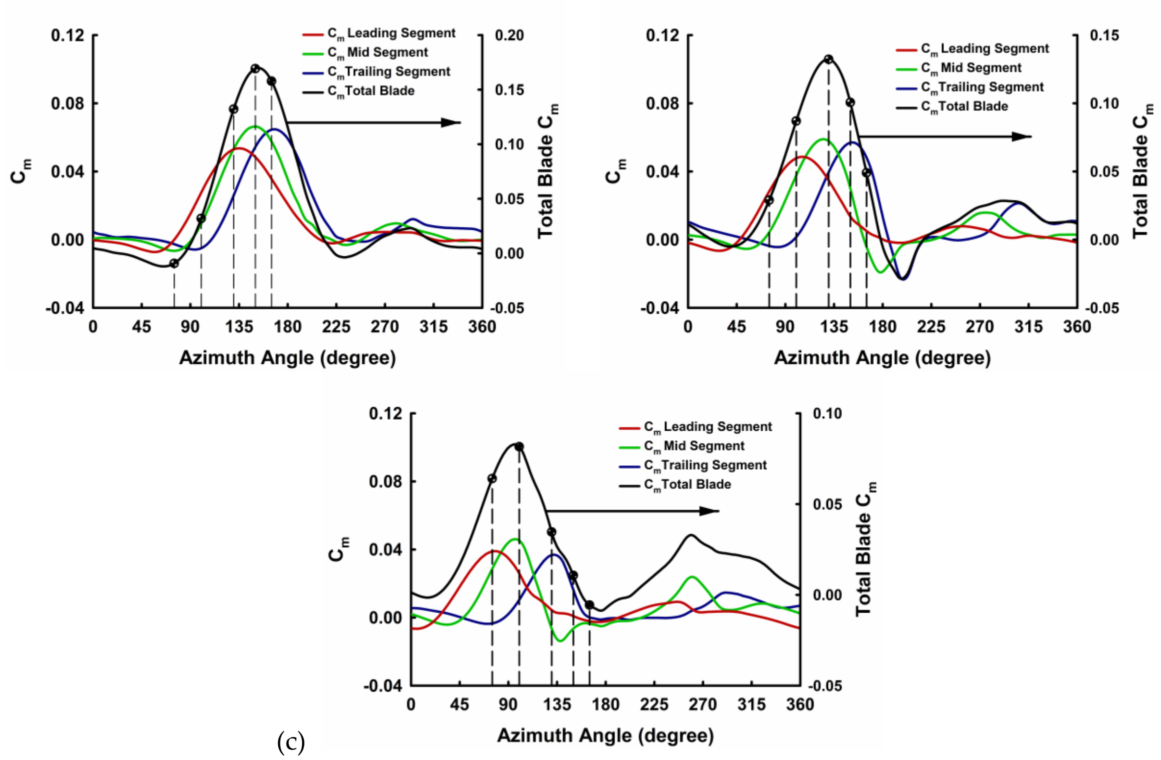

(c)

Figure 16. Section-wise Cm contribution of each segment of a single blade of (a) ϕ = 60°, (b) ϕ = 90° and (c) ϕ = 120° helical bladed VAWT operating at a TSR of 3.1

C_m contribution of each blade segment was observed over a rotation of 360°. The leading section, midsection and trailing section C_m is plotted in red green and blue colours respectively in figure 16. Figure (a), (b) and (c) represents the contribution curves of 60°, 90° and 120° respectively. The cumulative C_m is also plotted in the same plot with a different scale of y-axis in black colour. It is interesting to see that the midsection of the blade is contributing marginally higher than the other two sections in all helical bladed VAWT, for 90° and 60° helical bladed VAWT, the trailing section is contributing more to the moment coefficient when compared to the leading section. On the contrary, in 120° helical bladed VAWT, the leading segment contributes more than the trailing segment when operated in the same TSR of 3.1. It can be noticed from the figure that all sections of blades are not contributing uniformly to the moment coefficient. Drop lines are also plotted in figure 16 to highlight important azimuth angles. Corresponding to those azimuth angles the z-vorticity contours are plotted in figure 17-19. These points are of importance as they represent the peaks of individual segments of the same blade.

Figure 17-19 represents the z-vorticity contours of 60° (figure 17), 90° (figure18) and 120° (figure 19) helical blade VAWT at operating condition of TSR 3.1. It is essential to analyse the flow at different heights of the turbine as the cross section of the turbine varies along the height. Hence, the flow at different heights (-1.45m, -0.75m, 0m, 0.75m, and 1.45m) are analysed using these plots. Figure 16 represent the C_m curve of blade 1 which is represented in grey colour for figure 17-19. Blade 2 and Blade 3 are represented by brown and green colour respectively. At azimuth angle of 75°, 100°, 130°, 150° and 165° the contours are plotted. The vorticity levels are displayed to see the results of magnitude range of -50 to 50 s^{-1}. It is observed for a 60° helical blade VAWT, at θ = 130°, the leading edge of the leading segment of the blade starts forming vortices and this explains the peak for the leading segment of the blade observed in Figure 16. It is also observed that the leading edge

Preprints (www.preprints.org) | NOT PEER-REVIEWED | Posted: 7 December 2020 doi:10.20944/preprints202012.0140.v1

of blade 1 doesn't shed the vortices in any of the shown frames. The mid segment and trailing segment of Blade 1 starts developing leading edge vortices at θ = 150° and θ = 165° respectively and the same can be observed in figure 17 (d) and (e). Whereas it can be seen that the leading segment of Blade 3 sheds the vortices in figure 17(a) and in figure 17(e) the flow separation from the blade 3 can also be noticed. The separated flow from blade 2 can be seen in the figure 17 (a-e) interacting with blade 3 thereby creating the secondary peaks in the C_m plot. The vortex shed by the shaft is also visible in the figure and it combines with the flow shed by blade 2 in the downstream.

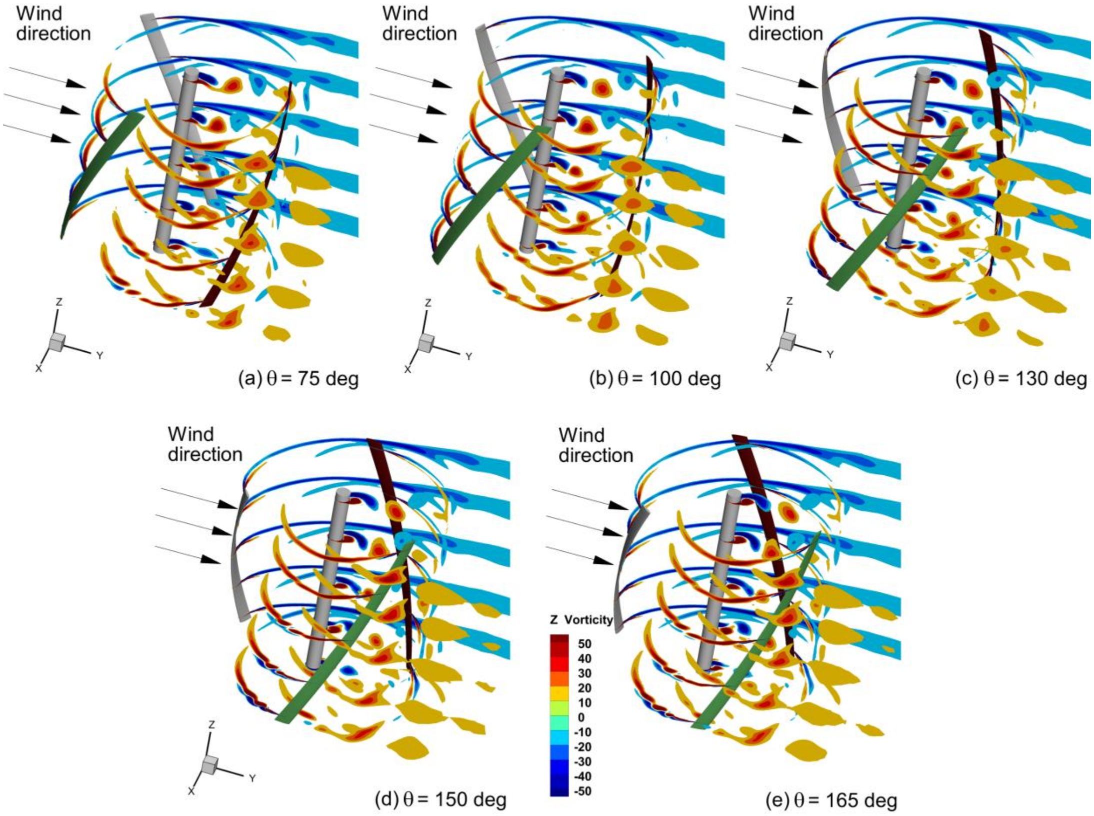

Figure 17. Z Vortex magnitude for 60° helical VAWT at z planes at height of -1.45m, -0.75m, 0m, 0.75m and 1.45m at azimuth angle of rotation of (a) 75°,(b) 100°,(c) 135°, (d) 150° and (e) 165°

The z-vorticity plots of 90° helical bladed VAWT is plotted in figure 18. At θ = 75° the leading edge vortices can be noticed on the leading segment of blade 1. This phenomenon happens to the trailing segment at much higher azimuth angle when compared to 60° helical bladed Turbine. The leading segment makes a peak at around θ = 100° and the interactions can be seen from figure 18(b) that the entire leading segment has entered the flow. The mid segment and trailing segment of the blade starts generating leading edge vortices at θ = 150° and θ = 160° of the azimuth angle. Mean while flow separation in the leading segment of the blade is noticed in the figure 18(d and e). Blade 2 can be seen interacting with the vortex shed by blade 1 at θ = 130°. The flow separations from blade 3 can be seen from θ = 130° (figure 18 (c)) and goes on to shed vortices for the trailing segment at θ = 165° (Figure 18(e)). The secondary interactions can be noticed by observing blade 3. It is seen interacting with the vortices shed by blade 2 as early as θ = 100°. The secondary interactions happen for longer azimuth angle of rotation and hence a wider secondary peak is observed for 90° helical bladed VAWT.

Preprints (www.preprints.org) | NOT PEER-REVIEWED | Posted: 7 December 2020 doi:10.20944/preprints202012.0140.v1

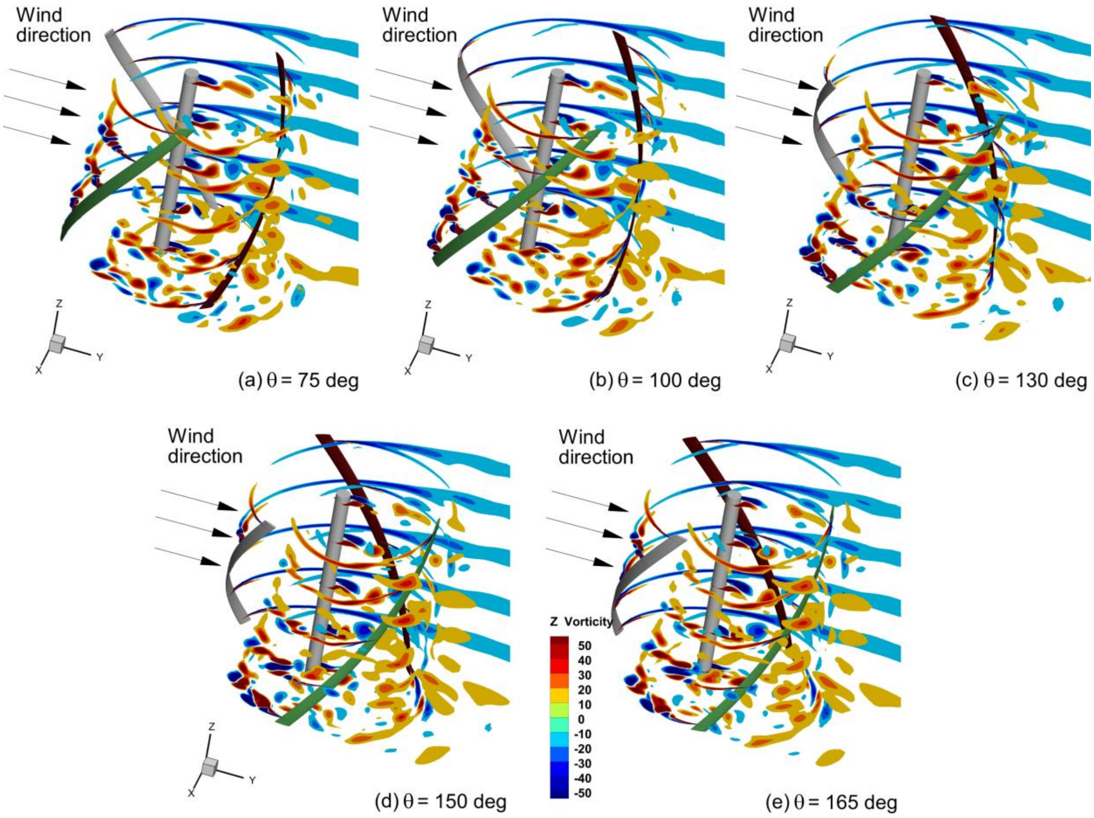

Figure 18. Z Vortex magnitude for 90° helical VAWT at z planes at height of -1.45m, -0.75m, 0m, 0.75m and 1.45m at azimuth angle of rotation of (a) 75°,(b) 100°,(c) 135°, (d) 150° and (e) 165°

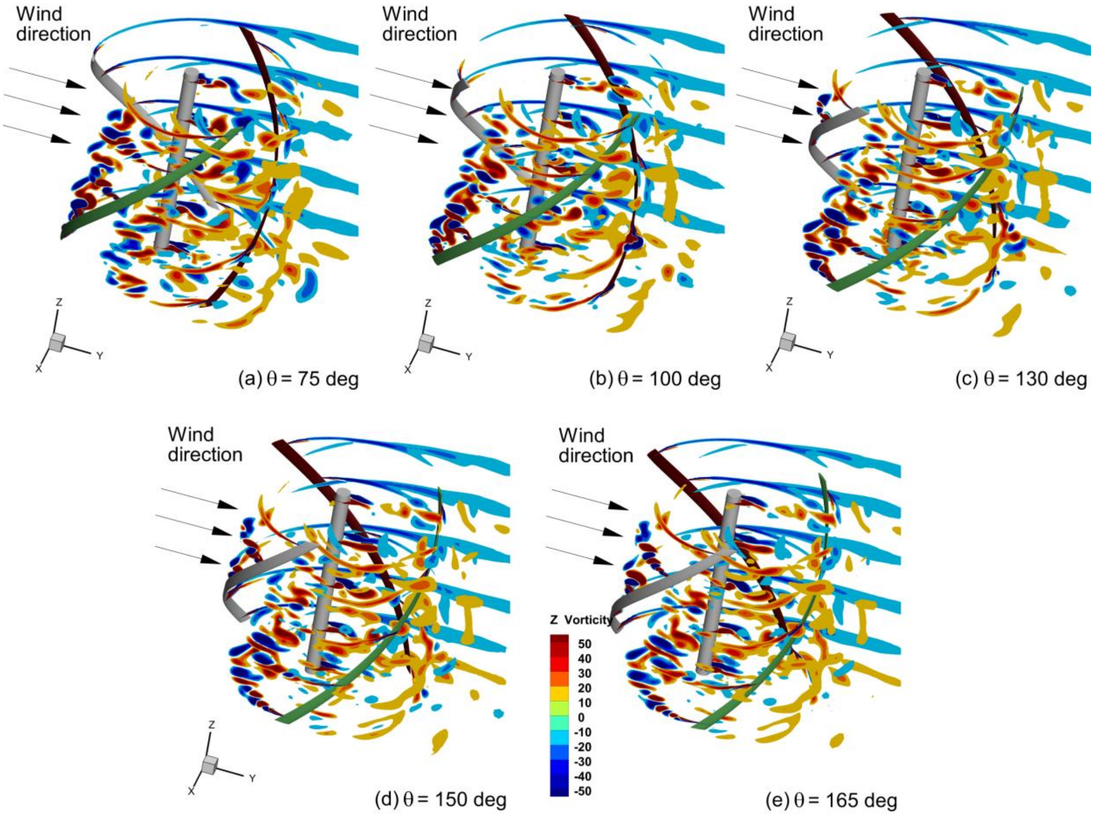

Figure 19. Z Vortex magnitude for 120° helical VAWT at z planes at height of -1.45m, -0.75m, 0m, 0.75m and 1.45m at azimuth angle of rotation of (a) 75°,(b) 100°,(c) 135°, (d) 150° and (e) 165°

For 120° helical bladed VAWT it can be seen that the leading segment has already entered the flow at θ = 75°. The leading segment of the blade can be seen interacting with the vortices of blade 3 at θ =

Preprints (www.preprints.org) | NOT PEER-REVIEWED | Posted: 7 December 2020 doi:10.20944/preprints202012.0140.v1

130° and starts shedding the vortices from the blade surface. The vortex shed by the blade 2 interacts with blade 3 and can be seen that the flow separation occurs at much earlier azimuth angles.
It can be seen from figures 17--19 that the flow interactions are higher for 120° helical blade when compared with other turbines. The blade 3 is coming under the secondary wake interactions produced by blade 2 at different sections of the blade. This explains the secondary peak observed in the C_m plot. It would be interesting to see the flow characteristics for various tip speed ratios. To study the same a 90° helical bladed VAWT's performance was observed. In figure 20, a 90° helical bladed VAWT was observed for the performance of different sections of the blade. As already observed from figure 7, the performance of the 90° helical bladed VAWT improves from TSR 2.7 to 3.1

To have a better understanding of how the blade sections behave with a change in TSR, 90 helical blade VAWT is studied for sectional contributions. From figure 17, it can be noted that the leading section is contributing less when compared to other sections of the same blade. For lower TSR, all three sections of the blade contribute an almost equal amount to the cumulative performance of the blade. At TSR 2.7 and 3.1, the secondary interactions are higher and seem to contribute positively towards the generation of power. At lower TSR the secondary peak is generated. Drop lines are plotted near to the peaks of each segment and analysed for flow vortices at various heights. The characteristics of individual C_m plot can be better understood when we look at the blade vortex generation and interaction.

(a)

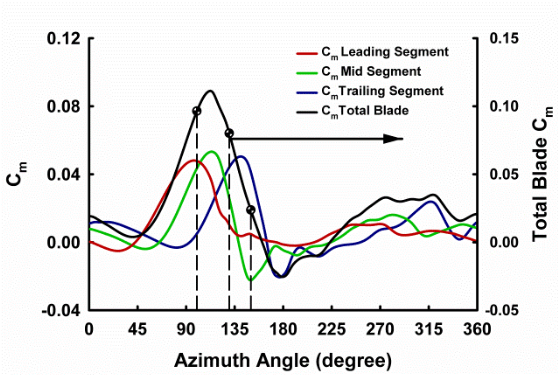

(b)

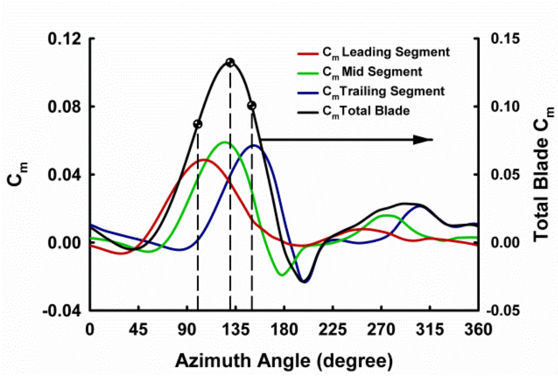

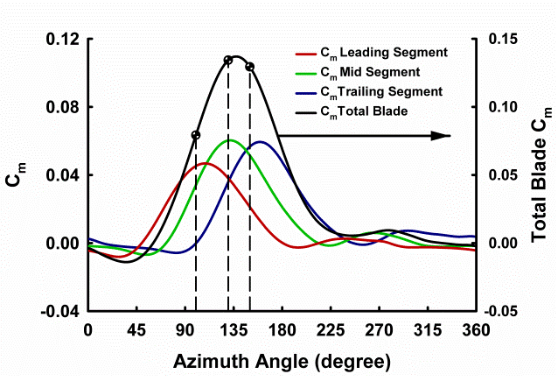

(c)

Figure 20. Section-wise C_m contribution of different segment of a single blade of a 90 helical VAWT operating at TSR (a) 2.7, (b) 3.1 and (c) 3.5

Figure 21 represents the z-vorticity contours of a 90° helical blade VAWT operating at TSR 2.7 (Figure 21 (a)-(c)), TSR 3.1(Figure 21 (d)-(f))and TSR 3.5 (Figure 21 (g)-(i)) at three different azimuth angle (100°, 130° and 150°) of rotation of blade 1. The colour notation used for the blades in figure 17-19 is used here as well. It can be seen that the flow separation happens in lower tip speed ratio there by increasing the interaction of the shed vortex on the receding blades. This substantiates the observation about the secondary peaks found in figure 20. The flow separations are found minimal in TSR3.5 there by producing better C_m when compared to other TSRs. It is also found that the z-vorticity generated by the shaft reduces as TSR increases.

Preprints (www.preprints.org) | NOT PEER-REVIEWED | Posted: 7 December 2020 doi:10.20944/preprints202012.0140.v1

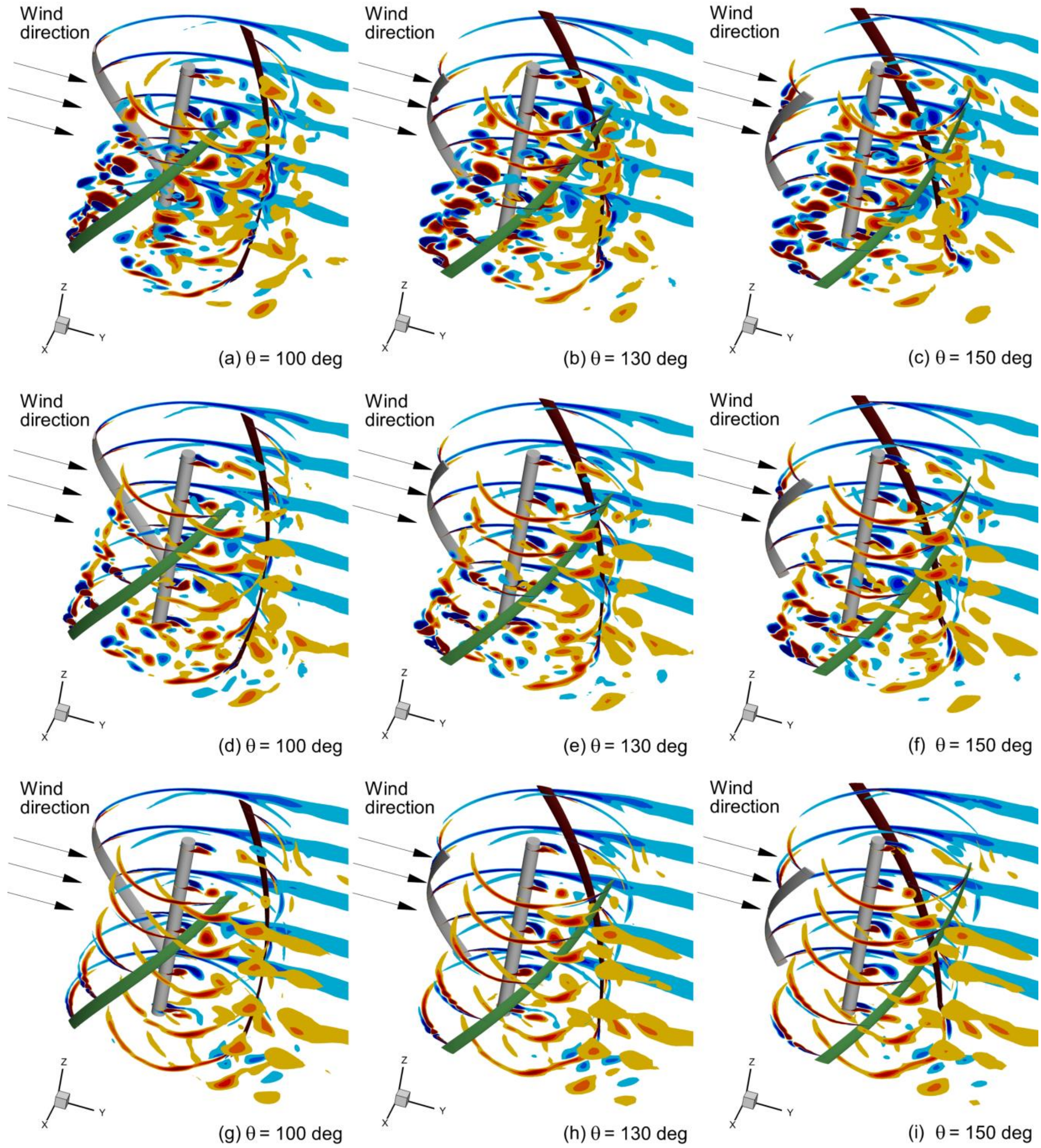

Figure 21. Z vorticity magnitude of 90° helical bladed VAWT at 100°, 130° and 150° of azimuth angle of rotation of turbine operating at (a-c) TSR = 2.7, (d-f) TSR = 3.1 and (g-i) TSR = 3.5

4.3. Effect of helix angle on turbine wake

ϕ	Y/D = 2	Y/D = 3	Y/D = 4
0°	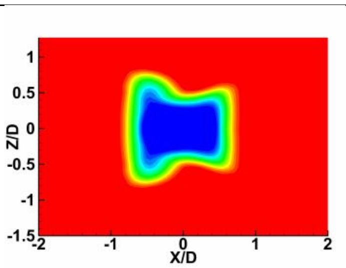	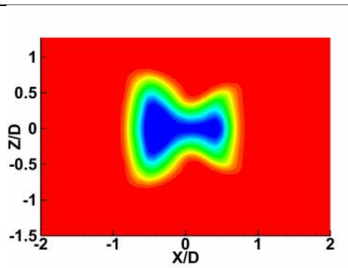	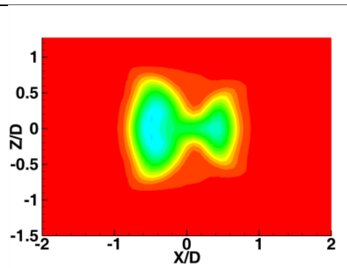

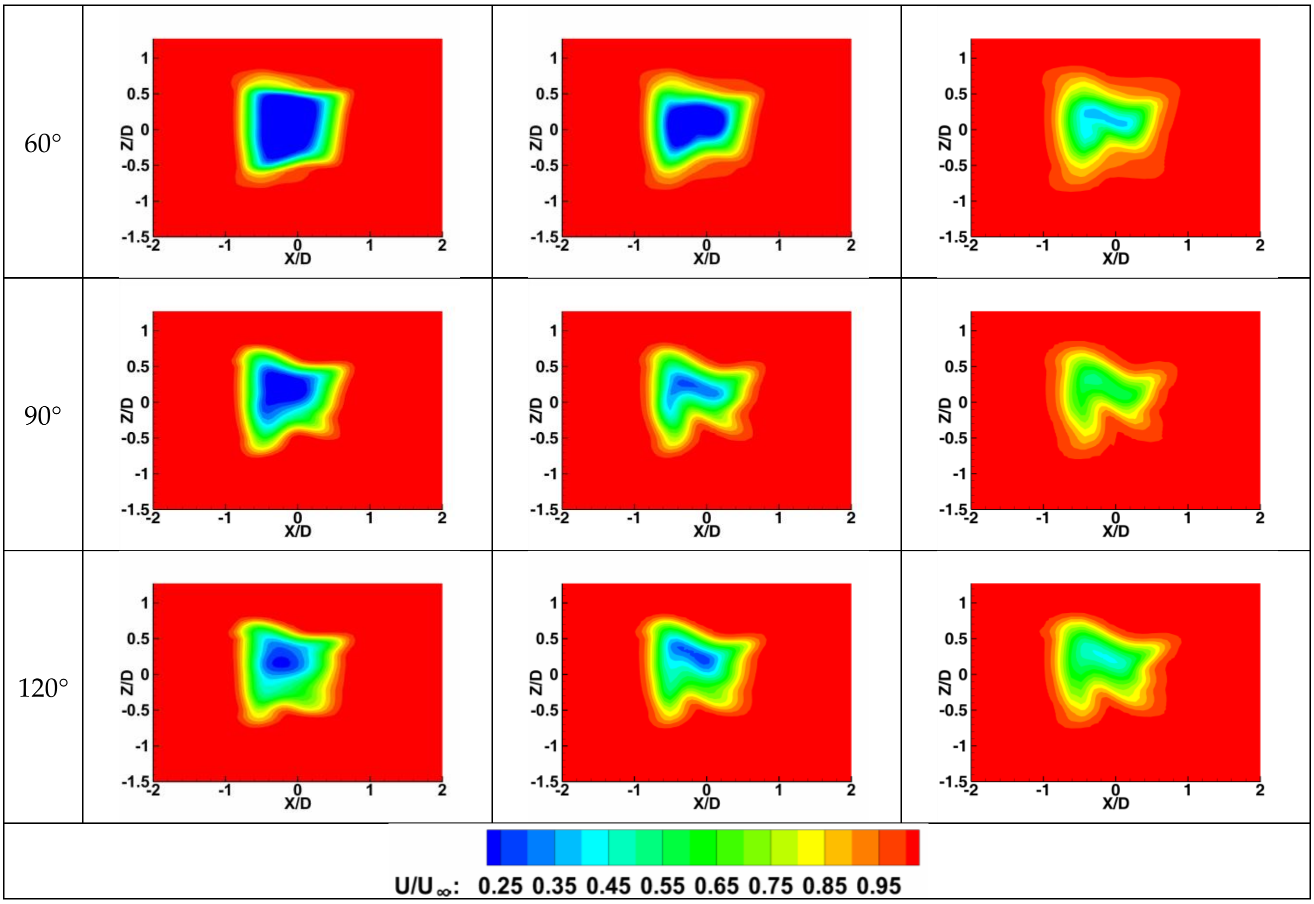

Figure 20. Wake structure of helical blade VAWT at Y/D of 2, 3 and 4. For straight and helical bladed VAWT at TSR = 3.1

Figure 20 and 21 presents the time-averaged (over the last turbine revolution) normalised stream-wise velocity along the non-dimensionalised lateral line, $-2 \le X/D \le 2$, at different down-stream locations in the turbine wake with Y/D = 2.0, 3.0, and 4.0, for λ= 3.1 (Figure 21) and 3.5 (figure 21). The scaling of the wake was followed based on the work done by Kadum et al.[46] The following points are observed:

- The turbine wake gets weaker at TSR 3.1 for 120° helical bladed VAWT when compared with straight and other helical turbines.
- The wake profile gets weaker when helix angle is increased even from a closer X/D rage of 2.
- The wake of helical bladed VAWT unlike straight blade seems to be dissipating quickly as helix angle increases. It further degrades when the tip speed ratio increases.

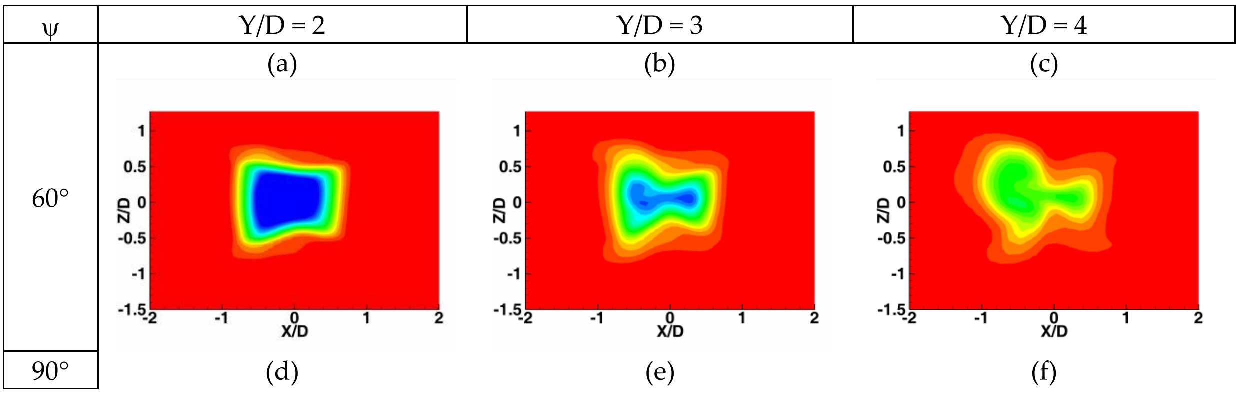

Preprints (www.preprints.org) | NOT PEER-REVIEWED | Posted: 7 December 2020 doi:10.20944/preprints202012.0140.v1

120°

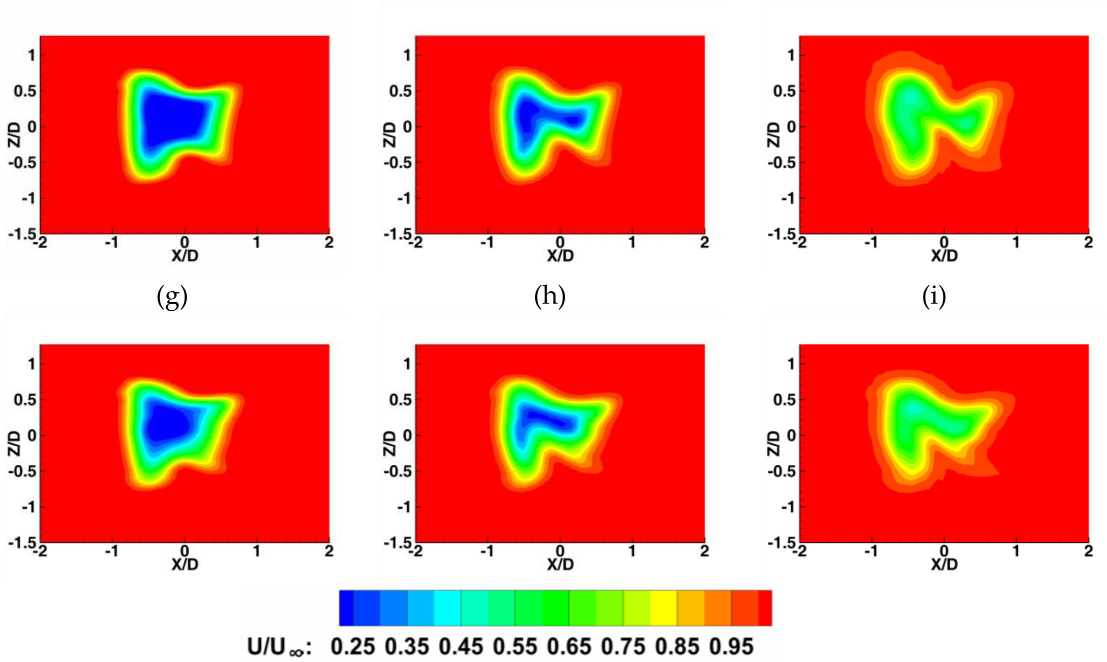

Figure 21. Wake structure of helical blade VAWT at Y/D of 2, 3 and 4. For helical bladed VAWT at TSR = 3.5

The turbine wake was studied in order to understand how the flow is going past the turbine. It is interesting to see how the wake dissipates over the length. Hence the wake characteristic for 90 helical blade VAWT is studied to understand the wake better. Figure 22 indicated the normalized wake characteristics for a 90 helical blade VAWT operating at TSR = 2.7, 3.1 and 3.5. This study is essential to understand how the flow past the turbine will behave as it also gives idea on how much of residual energy is left. The wake for 3.9 TSR at Y/D of 2, in comparison with other TSR the wake seems to have lost lot of energy. It is also noted that for the wake characteristic shapes remain almost similar a given Y/D for different TSR.

TSR	Y/D = 2	Y/D = 3	Y/D = 4
2.7	(a) 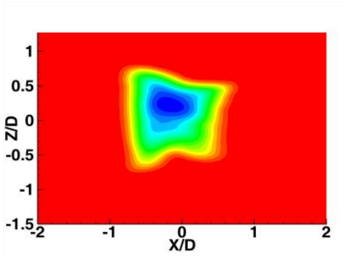	(b) 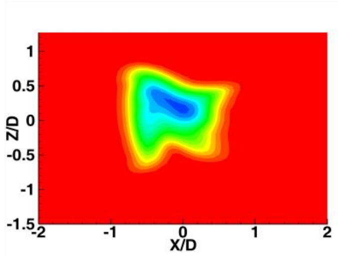	(c) 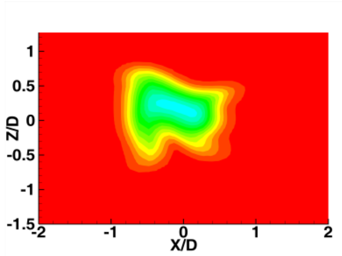
3.1	(d) 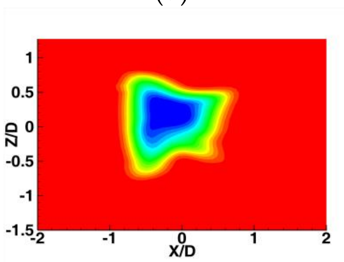	(e) 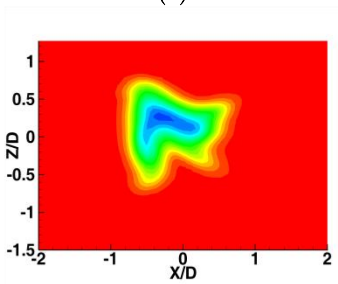	(f) 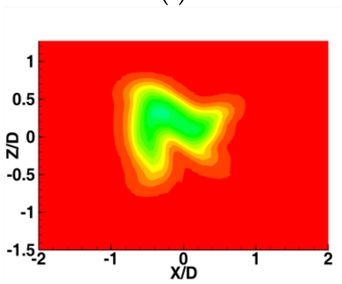

Preprints (www.preprints.org) | NOT PEER-REVIEWED | Posted: 7 December 2020 doi:10.20944/preprints202012.0140.v1

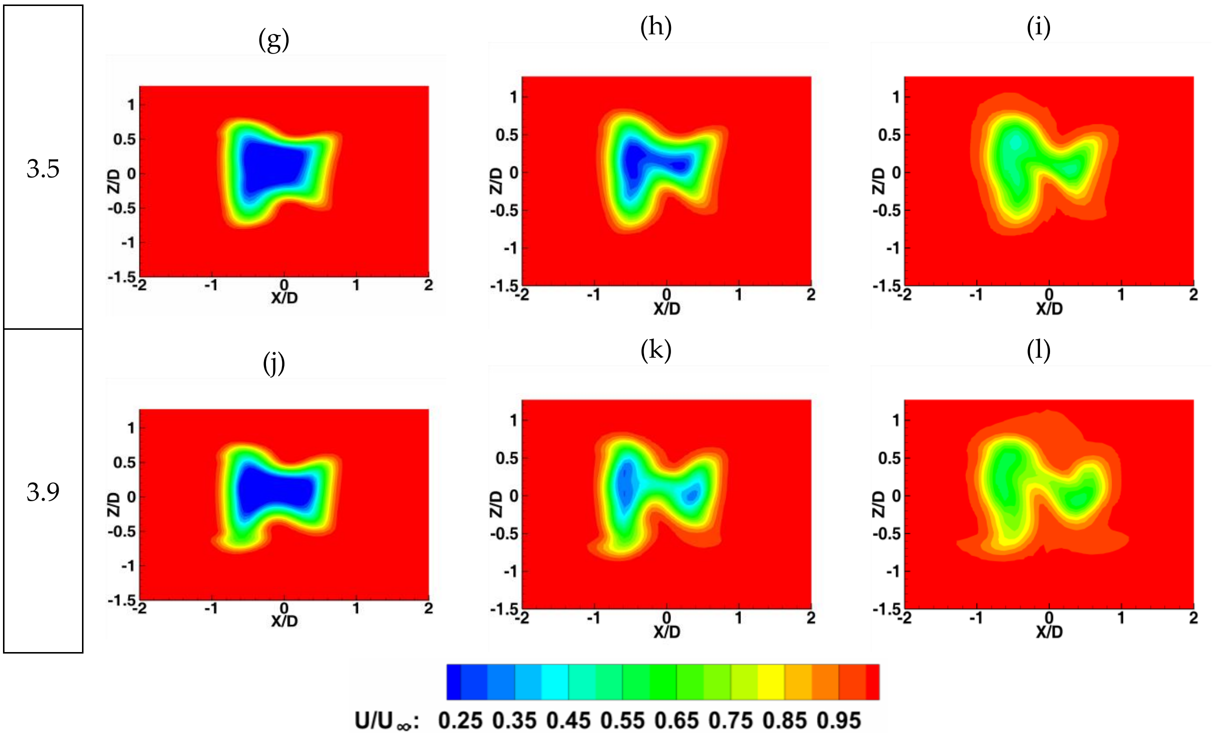

Figure 22 wake structure for a 90 helical bladed VAWT at Y/D of 2, 3, 4 and 6 operating at TSR of 2.7, 3.1, 3.5 and 3.9

5. Conclusions

In the present study effect of helix angles varying from 60° to 90° for helical VAWT have been studied. The turbine diameter is 2.7m and height 3m. 3D CFD model has been used to analyse the performance of these turbines. Following are the major conclusions derived from the work

- The study on effect of helix angle of a vertical axis wind turbine has shown that the performance, wake interaction and the flow interaction is different from a straight blade VAWT.
- The performance of a 60° helical blade VAWT was found to be out performing all the other VAWT blade shapes and had peak at a moderate TSR. However it had the highest standard deviation from average C_m produced by the turbine blade. Normalised C_m plots will enable to understand the moment coefficient characteristics.
- Analysing the quartile performance of the helical turbines, gave more insights on how the power production was distributed across the azimuth angle of rotation. The variation in the quartile performance is backed by the standard deviation plot which suggests that the minimum deviation is for 120° helical bladed VAWT. Since it has got the power production capabilities spread across the quartiles
- An essential detailed analysis of loads on the sections of blades revealed that the leading segment, mid segment and trailing segment of a single helical blade contributed different percentage of Cm to the cumulative blade Cm. Z-Vorticity contours at different heights of the turbine showed that the flow interference caused secondary peaks and also lead to better understanding of when and where the flow separation on the blade happens.
- In order to understand better the energy extraction a wake analysis was performed, leading to the understanding that wakes dissipate quickly for non-straight blade VAWTs.
- Effect of TSR on the performance of the turbine was also done with the help of a 90° helical bladed VAWT. Z-vorticity kept reducing as TSR increased from 2.7 to 3.5

Author Contributions: Conceptualisation, V. Ratna Kishore and Unnikrishnan D.; methodology, V. Ratnakishore, Unnikrishnan D.; software, V. Ratna Kishore, Akram Mohammed ; validation, V. Ratna Kishore and Unnikrishnan D.; formal analysis, V. Ratna Kishore; investigation, V. Ratna Kishore, Ajith Ramesh.; resources, Akram Mohammed.; data curation, Unnikrishnan D.; writing—original draft preparation, Unnikrishnan D.; writing—review and editing, V. Ratna Kishore, Ajith Ramesh; visualisation, Unnikrishnan D.; supervision, V. Ratna Kishore and Ajith Ramesh. All authors have read and agreed to the published version of the manuscript.", please turn to the CRediT taxonomy for the term explanation. Authorship must be limited to those who have contributed substantially to the work reported.

Funding: This research received no external funding

Acknowledgments: Would like to acknowledge the administration of Amrita Vishwa Vidyapeetham and King Abdul Aziz University of Science and Technology for the support extended for this work.

Conflicts of Interest: The authors declare no conflict of interest

References

1. Streck, C.; Keenlyside, P.; Von Unger, M. The Paris Agreement: a new beginning. *J. Eur. Environ. Plan. Law* **2016**, *13*, 3–29.
2. Agreement, P. *Report of The Conference of The Parties on Its Twenty-First Session, Held in Paris from 30 November to 13 December 2015*; FCCC/CP/2015/10/Add. 1, United Nations, European Commision Secretariate, 2015;
3. Savaresi, A. The Paris agreement: A new beginning? *J. Energy Nat. Resour. Law* **2016**, doi:10.1080/02646811.2016.1133983.
4. Delarue, E.D.; Luickx, P.J.; D'haeseleer, W.D. The actual effect of wind power on overall electricity generation costs and CO2 emissions. *Energy Convers. Manag.* **2009**, *50*, 1450–1456.
5. Kirthika, N.; Ramachandran, K.I.; Kottayil, S.K. Deep Quantile Regression Based Wind Generation and Demand Forecasts. In Proceedings of the International Conference on Soft Computing and Pattern Recognition; Springer, 2019; pp. 112–122.
6. Pedersen, E.; Persson Waye, K. Perception and annoyance due to wind turbine noise—a dose–response relationship. *J. Acoust. Soc. Am.* **2004**, *116*, 3460–3470.
7. Wagner, S.; Bareiss, R.; Guidati, G. *Wind turbine noise*; Springer Science & Business Media, 2012; ISBN 3642887104.
8. Crockford, N.J. *A review of the possible impacts of wind farms on birds and other wildlife*; Joint Nature Conservation Committee, 1992;
9. Tummala, A.; Velamati, R.K.; Sinha, D.K.; Indraja, V.; Krishna, V.H. A review on small scale wind turbines. *Renew. Sustain. Energy Rev.* **2016**, *56*, 1351–1371, doi:https://doi.org/10.1016/j.rser.2015.12.027.
10. Thönnißen, F.; Marnett, M.; Roidl, B.; Schröder, W. A numerical analysis to evaluate Betz's Law for vertical axis wind turbines.; IOP Publishing; Vol. 753, p. 22056.
11. Madsen, H.A.; Paulsen, U.S.; Vitae, L. Analysis of VAWT aerodynamics and design using the Actuator Cylinder flow model.; IOP Publishing; Vol. 555, p. 12065.
12. Gulve, P.; Barve, S.B. Design and construction of vertical axis wind turbine. *Int. J. Mech. Eng. Technol.* **2014**, *5*, 148–155.
13. Tjiu, W.; Marnoto, T.; Mat, S.; Ruslan, M.H.; Sopian, K. Darrieus vertical axis wind turbine for power generation II: Challenges in HAWT and the opportunity of multi-megawatt Darrieus VAWT development. *Renew. Energy* **2015**, *75*, 560–571.
14. Li, Q.; Maeda, T.; Kamada, Y.; Shimizu, K.; Ogasawara, T.; Nakai, A.; Kasuya, T. Effect of rotor aspect ratio and solidity on a straight-bladed vertical axis wind turbine in

three-dimensional analysis by the panel method. *Energy* **2017**, *121*, 1–9, doi:10.1016/j.energy.2016.12.112.
15. Li, Q.; Maeda, T.; Kamada, Y.; Murata, J.; Shimizu, K.; Ogasawara, T.; Nakai, A.; Kasuya, T. Effect of solidity on aerodynamic forces around straight-bladed vertical axis wind turbine by wind tunnel experiments (depending on number of blades). *Renew. Energy* **2016**, *96*, 928–939, doi:10.1016/j.renene.2016.05.054.
16. Eboibi, O.; Danao, L.A.M.; Howell, R.J. Experimental investigation of the influence of solidity on the performance and flow field aerodynamics of vertical axis wind turbines at low Reynolds numbers. *Renew. Energy* **2016**, *92*, 474–483, doi:10.1016/j.renene.2016.02.028.
17. Mantravadi, B.; Unnikrishnan, D.; Sriram, K.; Mohammad, A.; Vaitla, L.; Velamati, R.K. Effect of solidity and airfoil on the performance of vertical axis wind turbine under fluctuating wind conditions. *Int. J. Green Energy* **2019**, *16*, doi:10.1080/15435075.2019.1671408.
18. Rezaeiha, A.; Kalkman, I.; Blocken, B. Effect of pitch angle on power performance and aerodynamics of a vertical axis wind turbine. *Appl. Energy* **2017**, *197*, 132–150, doi:10.1016/j.apenergy.2017.03.128.
19. El-Samanoudy, M.; Ghorab, A.A.E.; Youssef, S.Z. Effect of some design parameters on the performance of a Giromill vertical axis wind turbine. *Ain Shams Eng. J.* **2010**, *1*, 85–95.
20. Chandramouli, S.; Premsai, T.P.; Prithviraj, P.; Mugundhan, V.; Velamati, R.K. Numerical analysis of effect of pitch angle on a small scale vertical axis wind turbine. *Int. J. Renew. Energy Res.* **2014**, *4*, 929–935.
21. Ferreira, C.S.; Geurts, B. Aerofoil optimization for vertical-axis wind turbines. *Wind Energy* **2015**, *18*, 1371–1385.
22. Bedon, G.; De Betta, S.; Benini, E. Performance-optimized airfoil for Darrieus wind turbines. *Renew. Energy* **2016**, *94*, 328–340, doi:10.1016/j.renene.2016.03.071.
23. Sengupta, A.R.; Biswas, A.; Gupta, R. Studies of some high solidity symmetrical and unsymmetrical blade H-Darrieus rotors with respect to starting characteristics, dynamic performances and flow physics in low wind streams. *Renew. Energy* **2016**, *93*, 536–547, doi:10.1016/j.renene.2016.03.029.
24. Rezaeiha, A.; Kalkman, I.; Blocken, B. CFD simulation of a vertical axis wind turbine operating at a moderate tip speed ratio: guidelines for minimum domain size and azimuthal increment. *Renew. energy* **2017**, *107*, 373–385.
25. Parker, C.M.; Leftwich, M.C. The effect of tip speed ratio on a vertical axis wind turbine at high Reynolds numbers. *Exp. Fluids* **2016**, *57*, 74.
26. Siddiqui, M.S.; Rasheed, A.; Kvamsdal, T.; Tabib, M. Effect of turbulence intensity on the performance of an offshore vertical axis wind turbine. *Energy Procedia* **2015**, *80*, 312–320.
27. Wekesa, D.W.; Wang, C.; Wei, Y.; Zhu, W. Experimental and numerical study of turbulence effect on aerodynamic performance of a small-scale vertical axis wind turbine. *J. Wind Eng. Ind. Aerodyn.* **2016**, *157*, 1–14.
28. Bhargav, M.; Kishore, V.R.; Laxman, V. Influence of fluctuating wind conditions on vertical axis wind turbine using a three dimensional CFD model. *J. Wind Eng. Ind. Aerodyn.* **2016**, *158*, 98–108.
29. Wang, Z.; Wang, Y.; Zhuang, M. Improvement of the aerodynamic performance of vertical axis wind turbines with leading-edge serrations and helical blades using CFD and Taguchi method. *Energy Convers. Manag.* **2018**, *177*, 107–121.

30. Battisti, L.; Brighenti, A.; Benini, E.; Castelli, M.R. Analysis of Different Blade Architectures on small VAWT Performance. *J. Phys. Conf. Ser.* **2016**, *753*, 62009, doi:10.1088/1742-6596/753/6/062009.
31. Han, D.; Heo, Y.G.; Choi, N.J.; Nam, S.H.; Choi, K.H.; Kim, K.C. Design, fabrication, and performance test of a 100-w helical-blade vertical-axis wind turbine at low tip-speed ratio. *Energies* **2018**, *11*, 1517.
32. Battisti, L.; Persico, G.; Dossena, V.; Paradiso, B.; Castelli, M.R.; Brighenti, A.; Benini, E. Experimental benchmark data for H-shaped and troposkien VAWT architectures. *Renew. energy* **2018**, *125*, 425–444.
33. Bedon, G.; Castelli, M.R.; Benini, E. Proposal for an innovative chord distribution in the Troposkien vertical axis wind turbine concept. *Energy* **2014**, *66*, 689–698.
34. Bedon, G.; Castelli, M.R.; Benini, E. Optimal spanwise chord and thickness distribution for a Troposkien Darrieus wind turbine. *J. Wind Eng. Ind. Aerodyn.* **2014**, *125*, 13–21.
35. Persico, G.; Dossena, V.; Paradiso, B.; Battisti, L.; Brighenti, A.; Benini, E. Time-resolved experimental characterization of the wakes shed by H-shaped and troposkien vertical axis wind turbines. *J. Energy Resour. Technol.* **2017**, *139*, 31203.
36. Divakaran, U.; Kishore, V.R.; Ramesh, A. Effect of wind speed on the performance of Troposkein vertical axis wind turbine. *Int. J. Renew. Energy Res.* **2019**, *9*, 1510–1521.
37. Tjiu, W.; Marnoto, T.; Mat, S.; Ruslan, M.H.; Sopian, K. Darrieus vertical axis wind turbine for power generation I: Assessment of Darrieus VAWT configurations. *Renew. Energy* **2015**, *75*, 50–67.
38. Bhuyan, S.; Biswas, A. Investigations on self-starting and performance characteristics of simple H and hybrid H-Savonius vertical axis wind rotors. *Energy Convers. Manag.* **2014**, *87*, 859–867.
39. Lee, Y.-T.; Lim, H.-C. Numerical study of the aerodynamic performance of a 500 W Darrieus-type vertical-axis wind turbine. *Renew. Energy* **2015**, *83*, 407–415.
40. Scheurich, F.; Fletcher, T.; Brown, R. The influence of blade curvature and helical blade twist on the performance of a vertical-axis wind turbine.; p. 1579.
41. Karimian, S.M.H.; Abdolahifar, A. Performance investigation of a new Darrieus Vertical Axis Wind Turbine. *Energy* **2020**, *191*, 116551.
42. Bianchini, A.; Ferrari, L.; Magnani, S. Start-up behavior of a three-bladed H-Darrieus VAWT: experimental and numerical analysis.; American Society of Mechanical Engineers Digital Collection; pp. 811–820.
43. Jagtap, M.; Navale, L. Twist Angle Analysis of Helical Vertical Axis Wind Turbine (Vawt) Using Q-Blade. *Int. J. Res. Publ. Eng. Technol.* **2017**, *3*, 2454–7875.
44. Lee, J.-H.; Lee, Y.-T.; Lim, H.-C. Effect of twist angle on the performance of Savonius wind turbine. *Renew. Energy* **2016**, *89*, 231–244.
45. Rezaeiha, A.; Montazeri, H.; Blocken, B. On the accuracy of turbulence models for CFD simulations of vertical axis wind turbines. *Energy* **2019**, *180*, 838–857.
46. Kadum, H.; Friedman, S.; Camp, E.H.; Cal, R.B. Development and scaling of a vertical axis wind turbine wake. *J. Wind Eng. Ind. Aerodyn.* **2018**, *174*, 303–311.